Novel and industrially applicable cooling element for photovoltaic bifacial modules

L.W.R Wix

Photovoltaic Materials and Devices group,
Electrical Sustainable Energy department,
Faculty of EEMCS,
TU Delft

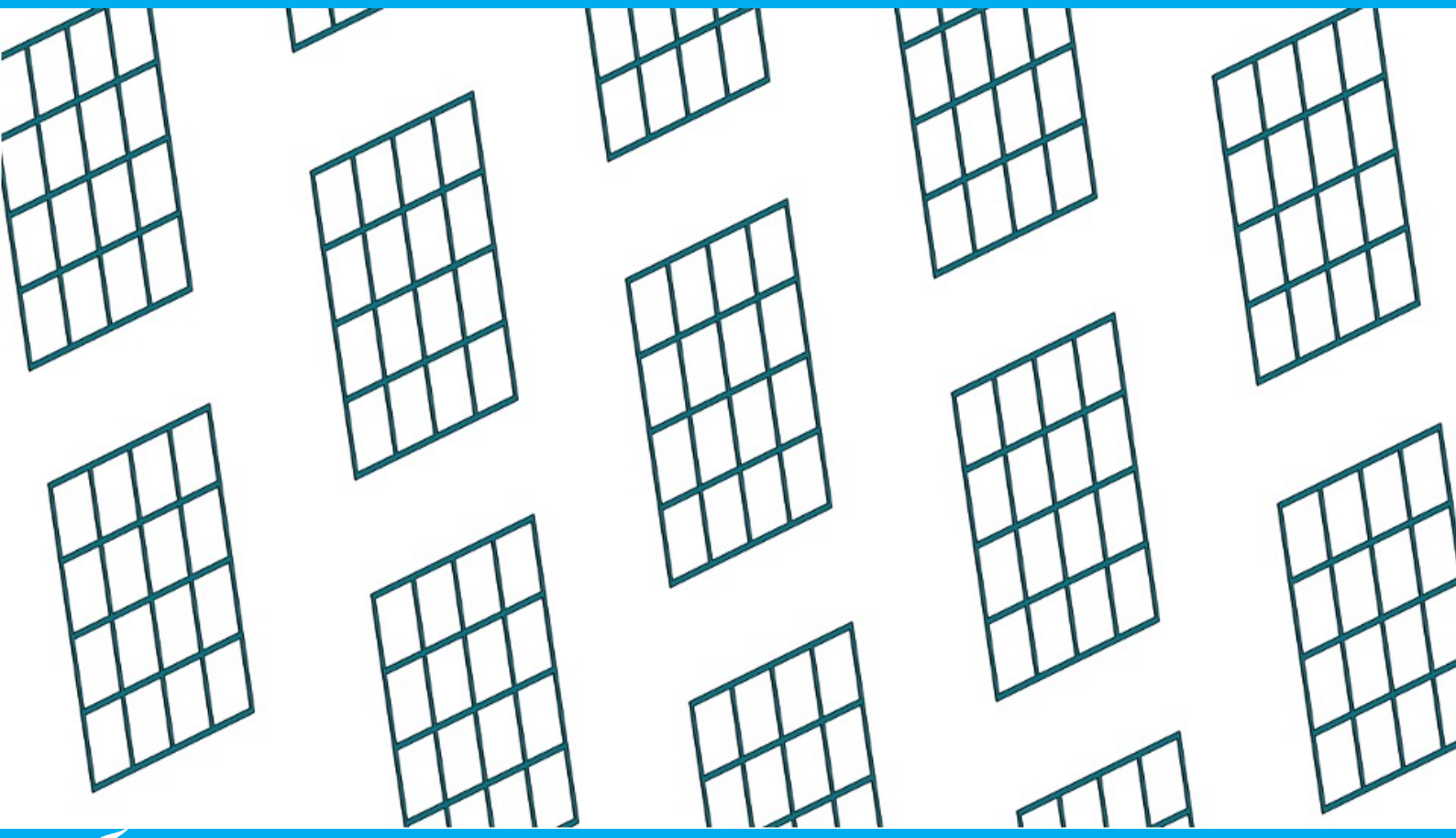

TU Delft

Novel and industrially applicable cooling element for photovoltaic bifacial modules

by

L.W.R Wix

to obtain the degree of Master of Science in Sustainable Energy Technologies
at the Delft University of Technology,
to be defended publicly on Tuesday March 18, 2021 at 10:00 AM.

Student number:	4270762	
Project duration:	November 12, 2019 – March 18, 2021	
Thesis committee:	Prof. dr. ir. O. Isabella,	TU Delft, ESE-PVMD, Supervisor
	Dr. H. Ziar.,	TU Delft, ESE-PVMD, Daily Supervisor
	Dr. P. Mangianello,	TU Delft, ESE-PVMD, Assistant Professor
	Dr. ir. M. Ghaffarian Niasar,	TU Delft, ESE-DCE&S, Assistant Professor
	ir. J.C. Ortiz Lizcano,	TU Delft, ESE-PVMD, PhD. Candidate

An electronic version of this thesis is available at `http://repository.tudelft.nl/`.

TU Delft

Preface

Ever since I was 15, I knew I wanted to venture into the sustainable energy field. Coming from Aruba, I saw the potential and possibilities of solar energy all around me. Now, 11 years later, I have obtained my masters degree in Sustainable Energy Technologies from the Delft University of Technology. In front of you lies my graduation thesis, "Novel and industrially applicable cooling element for photovoltaic bifacial modules". This journey did bring its challenges, however it was possible to rise above all of them thanks to a number of amazing people, to whom I would like to express my gratitude.

First, I would like thank my amazing and loving family. To my wonderful parents, Eduardo and Maybeline, and to my fantastic brother Lynrick, thank you so much for always believing in me, always inspiring me to chase my dreams and for always being my number one support system. Words cannot express the love I have for you. Thank you to my amazing cousins, Alexander and Daniëlle, for always being up to do something wild and for all of our fun moments together. To the rest of my big family in Aruba, Venezuela and Chile, thank you for always believing in me. And to my lovely grandmother Abe, thank you for being a beacon of strength and perseverance in my life.

I would like to express my gratitude to the PVMD group for the professional environment, cooperation and approachability. I would like to thank my supervisors, prof.dr.ir Olindo Isabella and dr. Hesan Ziar for their guidance, knowledge, insight and unwavering support throughout my thesis project. I would also like to thank Juan Camilo Ortiz-Lizcano, Andres Calcabrini, dr.ir Rudi Santbergen and dr. Malte Vogt for always lending me their knowledge. I also would like to thank Sander Bezuijen from COMSOL NL. This thesis would not have been possible without your immense help and insight.

To my amazing friends who have filled my student life with unforgettable moments. Celine, thank you for our hilarious high school days, for always being in my corner cheering me on and for all of our crazy (shopping) adventures during our studies. Maik, thank you for all your support and humor throughout our hectic bachelor days, our minor-program days an our SET days. Tessa, thank you for all your support, crazy karaoke challenges and for your wild hilariousness.
To my great friends from the best badminton club in Delft, United Shuttles Smashing Right, especially Pauline, Vincent, Abhishek and Prachi, thank you so much for all your support and unforgettable moments. I will cherish them forever. Nick, thank you for being a source of comedy and for our long and talkative walks.
To my amazing officemates of LB02.500, Martijn, Patrycja, Abdallah and Mohammed, thank you for all the hilarious moments we shared together and making our office an amazing workplace.

Lastly, I would like to thank my past self, for always persevering in the moments you felt like you couldn't, for always having the strength on the days you felt weak, for always having hope and for always and forever believing in yourself. You did it.

L.W.R Wix
March 18th, 2021
Delft

Abstract

Rising global temperatures have shifted mankind's methods of energy production towards a more sustainable manner. Solar energy technologies have become one of the world's leading methods of producing clean, sustainable energy. However, this technology has been facing some adversities in the field of thermal management. The majority of solar modules in the commercial market are monofacial modules, for which many thermal management solutions exist. For bifacial solar modules, this field is still being researched. This, together with the fact that bifacial modules are projected to reach a 40% market share by the year 2028, prompts the need for thermal management solutions for this technology.

The proposed solution is an integrated heat sink (IHS) built in a bifacial solar module. This was thoroughly researched using the multiphysics, FEM-based software COMSOL. The geometry was drawn using the COMSOL environment and a hybrid mesh was created to accommodate the module. Initial issues and computation errors led to decreasing of model dimensions. A 1 cm by 1 cm glass bifacial module was created and debugged successfully. This model was then simulated using two COMSOL studies: 'Heat Transfer in Solids' and 'Surface-to-Surface Radiation'. All of these simulations were performed using four illumination combinations (front illumination/back illumination [W/m^2]): 1000/50; 1000/100; 1000/200 and 1000/300. After successful simulations of the 1 cm by 1 cm model, the model was scaled up to a 4 by 4 (67.31 cm by 67.31 cm) glass bifacial module.

The results for both the 1 cm by 1 cm module and the 4 by 4 module were promising. In the case of 1000 W/m^2 front illumination and 300 W/m^2 back illumination, the 1 cm by 1 cm solar cell showed a temperature drop of 0.92°C and a relative efficiency gain of 0.359%. The solar cells in the 4 by 4 module showed a temperature drop of 1.33°C and a relative efficiency gain of 0.519%. Next, temperature simulations were performed with varying IHS thickness, from 1 mm to 10 mm. Taking into consideration that with increase thickness the temperature did not reduce significantly and that the module weight was being increased, a 1 mm IHS was found to be the most beneficial. Yield calculations were performed on a 2 by 2 (34.29 cm by 34.29 cm) bifacial module, both with and without the utilization of the IHS. It was found that with the utilization of the IHS, the financial gain was 0.05 €/m^2/year. Lastly, lifetime prediction analyses were performed to receive insight on the effect of the IHS on the lifetime of a bifacial module. It was found that the lifetime gain for a bifacial module with the IHS is about 26 days, corresponding to a relative lifetime gain of 0.68%. It should be noted however, that the lifetime of a module without the IHS under the simulation conditions was 10.27 years, far below commercially reported lifetimes. This is due to a high maximum operational temperature and a large difference between the minimum and maximum operational temperature.

The proposed integrated heat sink showcased positive effects in temperature management and efficiency gain in bifacial solar modules. The use of a hybrid mesh proved beneficial for the computation time and different scenarios can now be simulated. However, yield calculations only showed a very small financial gain and lifetime prediction analyses showed a very small lifetime gain. Further improvements include a design that can increase the heat transfer of the IHS, such as varying the thickness of the bottom glass layer or utilizing a transparent backsheet. The possibility of connecting the IHS to the frame of the module to further increase the heat transfer to the environment should be investigated. Also, different material options for the IHS and the addition of heat dissipation fins should also be researched.

Contents

1 Introduction

The main goal of this chapter is to give an introduction on solar energy and bifacial solar modules. Firstly, the necessity of renewable energy is discussed alongside the history of solar cells and modern standard test conditions criteria. Then, information on bifacial solar modules is presented. Lastly, the objective and outline of this thesis is given.

1.1. Background

In recent history, the human energy consumption has increased due to the enormous growth in population. The world population reached 7.7 billion people in 2019 and this number is expected to grow to 9.7 billion by the year 2050 [1]. Increased population is directly coupled with an increased energy consumption, which brings adversities to humankind on a global scale. The current energy infrastructure is highly dependent on the utilization of fossil fuels. Due to increased energy consumption, this is leading to a higher extraction rate compared to the production rate. Complete depletion of global reserves is inevitable, which makes fossil fuels a non-renewable energy source. As the global reserves decrease and energy consumption increases, an increase in global energy prices is approaching. Another issue of the utilization of fossil fuels is the large quantity emissions of greenhouse gasses. These emissions lead to an increased concentration of CO_2, CH_4 and NO_x in the atmosphere, further contributing to global warming. Rising global temperatures are a direct consequence, with a predicted 2°C global rise by the year 2065. This can be seen in figure 1.1.

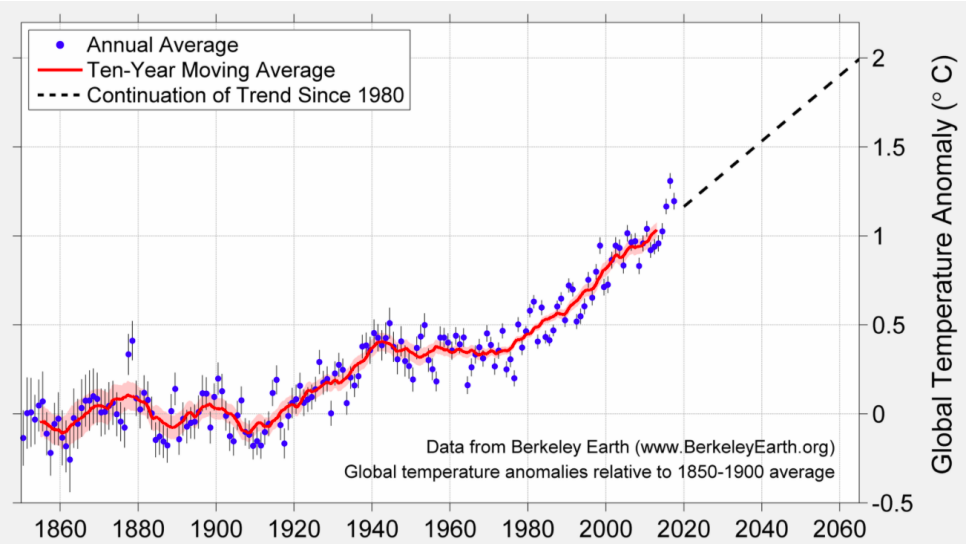

Figure 1.1: Ten-year moving average of Earth's surface temperature. Dotted line indicates the projected rise of global temperatures based on a trend that has been applicable since 1980 [2].

To tackle these adversities, a global shift to renewable energy sources is needed. An example of this is solar energy, which is the conversion of solar light into electricity by the use of semiconductor materials. This form of energy conversion is known as photovoltaic (PV) technology. Solar energy has become one of the most studied and most important renewable energy sources. How this energy is formed and harvested is as follows.
Due to nuclear fusion in the core of our Sun, energy is produced and transmitted to the surface of the Sun and then reaches the surface of the Earth as thermal radiation. This thermal radiation can be harvested using solar cells, which generate energy based on the photovoltaic effect [3]. However, not all of the thermal radiation can be harvested. Light scattering and absorption by aerosols, dust particles and air molecules reduces the radiation to a fraction of the emitted radiation. Furthermore, the Earth's location relative to the Sun and the geolocation of the harvest area has influence on the final radiation intensity [3].

The history of the solar cell is one that spans 182 years. In 1839, Alexandre Becquerel first observed the photovoltaic effect via an electrode in a conductive solution exposed to light [4]. Then, in 1883, Charles Fritts developed the first solar cell using selenium on a thin layer of gold, reporting an efficiency of less than 1%. The science behind the photovoltaic effect was published by Albert Einstein in 1905 and can be divided into three processes [3]:

1. **Generation of charge carriers.** In this stage, electrons absorbs energy received from photons (E_{ph}) that excites the electrons from their initial energy level, E_i, to a higher energy level E_f. However, this energy can only be absorbed if the electron energy levels are present so that their difference equals the photon energy (equation 1.1). Here is h the Planck constant and υ the frequency of the light.

$$E_{ph} = h\upsilon = E_f - E_i \tag{1.1}$$

   In an ideal semiconductor, electrons can occupy the energy levels below the valence band edge, E_V, and the energy levels above the conduction band edge, E_C. Between these two bands, no allowed energy states are to exist. This difference in energy is called the bandgap, $E_G = E_C - E_V$. Photons with energy smaller than the bandgap energy will not be absorbed in an ideal semiconductor. Next, if and when electrons are excited from E_i to E_f, voids are created at the initial energy level E_i. These voids will behave live positively charged particles, called holes. The process of photon energy absorption by electrons therefore leads to the creation of electron-hole pairs.

2. **Separation of charge carriers.**To utilize the energy stored in these newly created electron-hole pairs in an external circuit, semipermeable membranes are placed on both sides of the absorbing semiconductor. These membranes will ensure that electrons will only flow through one membrane and that the holes will only flow through the other membrane. These membranes are generally formed by negative-type and positive-type materials. However, these charge carriers must reach the membranes before they are able to recombine, which limits the thickness of the absorbing semiconductor.

3. **Collection of charge carriers.** At this step, the charge carriers can be extracted from the solar cells with the utilization of electrical contacts so work can be performed on an external circuit. Once passed through the circuit, the electrons will recombine with the holes at a metal-absorber interface.

In 1954, the American Bell laboratories announced the invention of the first modern silicon solar cell [4]. This lead to many laboratories across the globe researching, creating and testing solar cells. Since then, solar cell research and development have only increased. To ensure proper and correct comparison of different solar cell technologies, standard test conditions were introduced [3]. These conditions are characterized by:

- Standard incident irradiance of 1000 W/m^2
- AM1.5 spectrum
- Cell temperature of 25 °C

The AM1.5 spectrum is the reference solar spectrum distribution defined by the International Standard IEC 60904-3 [5]. This AM1.5 spectrum is from the solar irradiance received on a plane tilted at 37° to the horizontal, facing the Sun. The total irradiance of the AM1.5 spectrum is 1000 W/m^2, which is close to the maximum irradiance received on the Earth's surface on a cloudless day. This spectrum alongside other spectra can be seen in figure 1.2. AM stands for 'Air Mass', which is the ratio between the distance that the sunlight has to travel to reach a certain location and the minimal possible path when the Sun is at the zenith.It should be noted that the AM0 spectrum is the irradiance distribution outside the Earth's atmosphere.

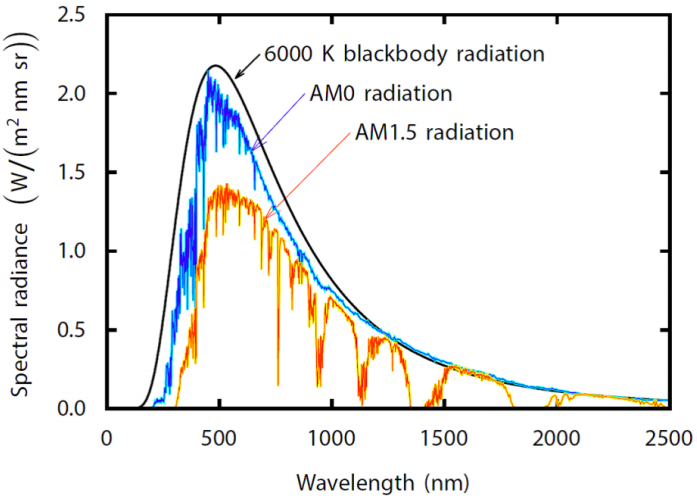

Figure 1.2: Three solar spectra. The black curve represent the spectrum of a blackbody with a temperature of 6000 K. The blue curve represents the AM0 spectrum and the orange curve represents the AM1.5 spectrum [3].

1.2. Bifacial solar modules

When solar cells were being researched and developed, a new technology was discovered: bifacial solar cells. The main characteristic of bifacial technology is, as the name suggests, the ability to capture light from both sides of the solar cell. The rear side of a bifacial module receives less irradiance in comparison to the front side. This is why the albedo of the surrounding area is of utmost importance in bifacial solar installations. Higher albedos offer higher reflectivity, effectively increasing the the irradiance that reaches the rear side of the module and thus increasing power production.
The history of bifacial solar cells starts around the same time as the invention of the first modern silicon solar cell. In 1960, Hiroshi Mori first proposed the bifacial solar cell [6]. Then, in 1977, the first publications regarding bifacial solar cells appeared at the first European Photovoltaic Solar Energy Conference. A device with an 7% efficiency was presented by two research groups from Mexico and Spain [6]. Ever since, while monofacial cells were being researched and were made the most accessible of the two technologies, bifacial solar technologies never ceased to be researched and developed. Many studies have been carried out and with these studies, new concepts were introduced. One such concept is the bifaciality factor, which is the ratio between the absorbed power between the rear side and front side of the module (equation 1.2).

$$f_B = \frac{P_{rear}}{P_{front}} \tag{1.2}$$

Another important parameter is the bifacial gain (BG), which can be calculated using equation 1.3 and is described as the ratio of the bifacial module energy yield (Y_b) over the monofacial module energy yield (Y_m) in the same location with the same optimal orientations [7].

$$BG = \frac{Y_b}{Y_m} - 1 \tag{1.3}$$

According to the ITRPV report of 2020 [8], the world market share of bifacial solar technology has been increasing, which can be seen in figure 1.3. With a projected market share of 35% by the year 2030, bifacial technology offers a promising broadening of PV technologies and an immense contribution to solar energy harvesting. Bifacial solar modules experience the same adversities as monofacial solar modules when it comes to module operation. High temperatures have a negative impact on solar cell performance, which will be described in chapter 2. Many current thermal solutions are focused on monofacial modules, while thermal solutions for bifacial modules are still in research. The bifacial solar technology share is ever increasing and this technology offers the possibility of increased solar energy harvesting. It is for these reasons that further research is needed on the thermal management aspect of this technology to further improve and increase energy yields.

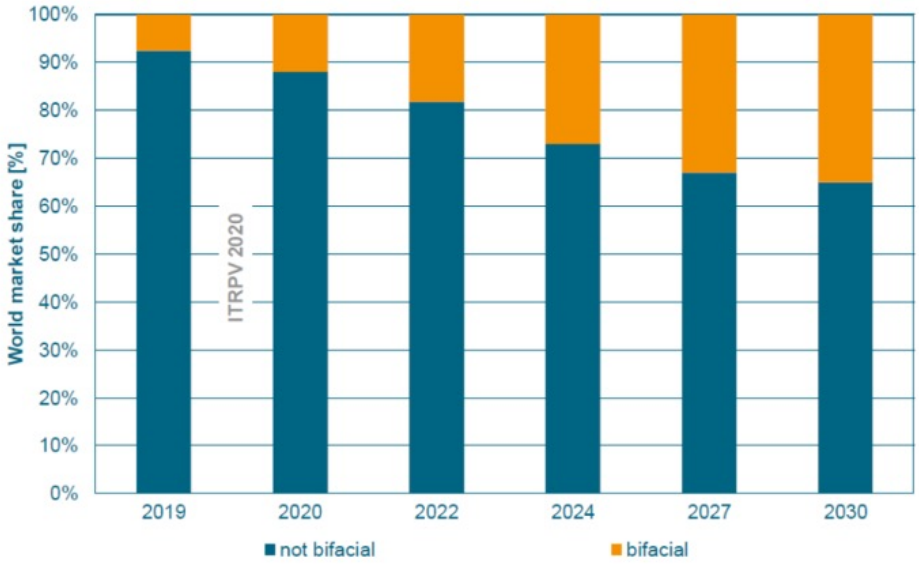

Figure 1.3: Projected bifacial solar technology market share [8].

1.3. Thesis objective and outline

There are multiple solutions for the thermal management of PV modules, however many of the current solutions are for monofacial PV modules. Thermal management for bifacial PV modules is still a relatively new field that is still being researched. One of many thermal management solution, which are heat sinks, have already been researched and applied for monofacial PV modules. However an integrated heat sink for a bifacial solar module where no optically active area is lost has not yet been designed and researched. The objective of this thesis is to reduce the operational temperature of bifacial PV modules with the inclusion of an integrated heat sink (IHS), thereby increasing the electrical efficiency.

This thesis is divided into five chapters. In this chapter, an introduction on solar energy is presented. Additionally, bifacial solar modules are introduced alongside their history, increasing market share and future outlook.

Chapter 2 discusses the electrical properties of solar cells as well as the temperature effects on solar cell operations. An explanation as to why increased operating temperature has a negative impact on solar cell operation is given. Furthermore, some current thermal management technologies are presented.

In chapter 3, the simulation models used in this thesis are introduced. The model geometry is presented and heat transfer mechanisms that occur during PV module operation are given. Next, a detailed, multiphysics description is presented of the model created and simulated in COMSOL. Furthermore, an description on how yield calculations and lifetime prediction analyses were conducted is given.

Chapter 4 encompasses the results obtained from the thermal simulations conducted in COMSOL. Yield calculation results and lifetime prediction results are also presented next to result discussions.

Lastly, in chapter 5, the conclusions of this research are summarized and the outlook and recommendations for future research are given.

2

Temperature effects on solar cells

In this chapter, the effects on temperature on solar cells are discussed. Firstly, electrical properties of solar cells are presented. Next, how (increased) temperature affects these properties are discussed and lastly, current thermal management solutions for PV modules are presented.

2.1. Electrical properties of solar cells

During solar cell operation, about 15 to 20% of the incident irradiation is converted into electricity, while the remaining 80% is converted into heat [9]. The overall electrical efficiency is thus heavily influenced and limited by the operating cell temperature, which in turn is influenced by heat production. When manufacturers perform test on newly produced solar cells, they are tested using standard test conditions.
Manufacturers make data sheets available that contain important information of their solar modules. One of the most important set of information are the electrical properties of a solar module characterized by electrical parameters. These parameters are as follows:

- **Short circuit current (I_{sc})**. This is the current that flows through the external circuit when the electrodes of a solar cell are short circuited. The short circuit current is depended on the incident photon flux, determined by the spectrum of the incident light [3].
- **Open-circuit voltage (V_{oc})**. This represents the voltage at which no current flows through the external circuit. This corresponds to the maximum voltage a solar cell is able to deliver [3].
- **Fill factor (FF)**. The fill factor is defined as the ratio between maximum power generated by the solar cell and the product of V_{oc} and I_{sc}. The maximum power is represented by P_{mpp} and calculated by the product of the maximum voltage and maximum current ($P_{mpp} = V_{mpp} I_{mpp}$). Here, 'MPP' denotes the maximum power point, which is a point on the I-V curve of the solar cell at which maximum power is produced. The fill factor is calculated using equation 2.1 [3].

$$FF = \frac{P_{mpp}}{V_{oc} I_{sc}} = \frac{V_{mpp} I_{mpp}}{V_{oc} I_{sc}} \tag{2.1}$$

- **Conversion efficiency (η)**. The conversion efficiency is defined as the ratio between the maximal generated power and the incident power on the solar cell. This can be calculated using equation 2.2 [3].

$$\eta = \frac{P_{max}}{P_{in}} = \frac{V_{mpp} I_{mpp}}{P_{in}} = \frac{V_{oc} I_{sc} FF}{P_{in}} \tag{2.2}$$

A typical I-V and P-V curve for a solar cell can be seen in figure 2.1. Another important parameter for thermal management of solar cells is the temperature coefficient with respect to the efficiency. This coefficient indicates by how much the efficiency drops for each whole increment of temperature above the standard test condition temperature. This coefficient is usually given in %/°C.

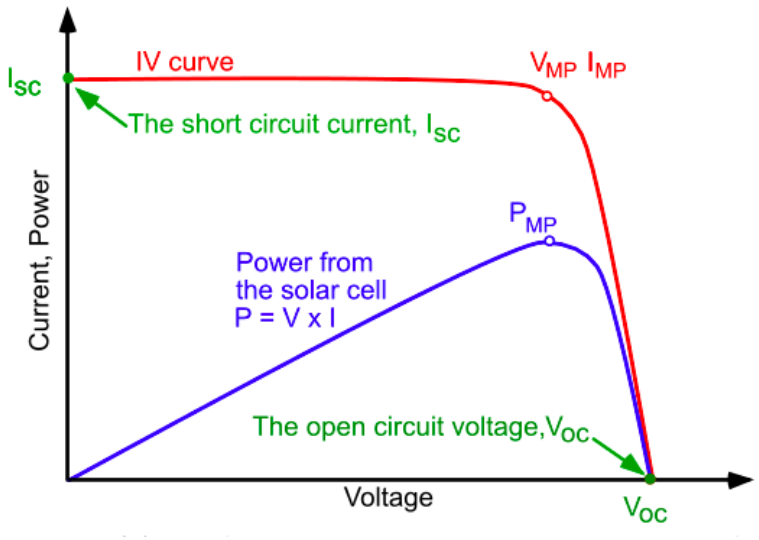

Figure 2.1: Typical I-V curve (shown in red) and P-V curve (shown in blue) for a solar cell [10].

2.2. Temperature Effects on Solar Cell Operations

Solar cells operate in an open environment, which is heavily influenced by ambient properties. Ambient temperature can have a negative impact on the maximum power that a solar cell can produce. This is visualized in figure 2.2.

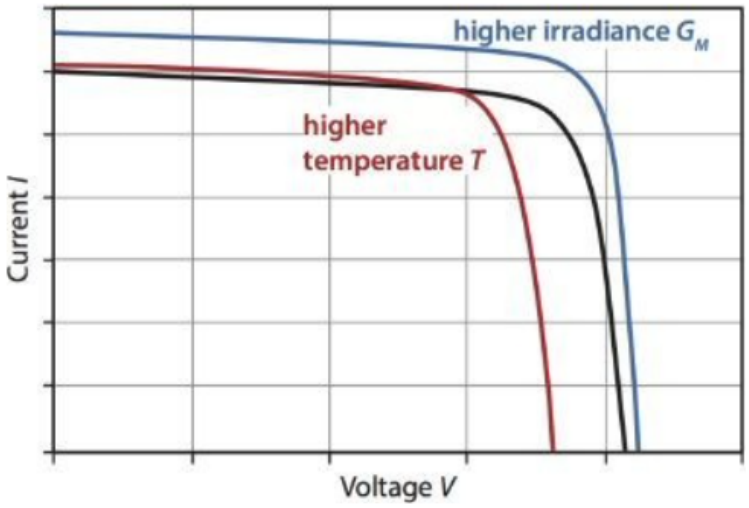

Figure 2.2: Temperature and irradiance effect on solar cell I-V curve [3].

There are three curves in figure 2.2. The black curve represents a standard I-V curve. The blue curve represents the effects of increased irradiance (denoted as G_M). This results in a higher V_{oc} and a higher I_{sc}. The effect of increased cell temperature can be seen by the red curve. It can be seen that the I_{sc} increases slightly, but the V_{oc} decreases dramatically. This effectively reduces the fill factor and ultimately the efficiency. How this occurs physically and mathematically is as follows.
The primary effect of a decrease in V_{oc} for higher temperatures is due to an increase of intrinsic carrier concentration, which leads to a higher saturation current density [3]. This phenomenon can be explained with equation 2.3.

$$V_{oc} \approx \frac{nk_BT}{q} \ln\left(\frac{J_{sc}}{J_0}\right) = \frac{nk_BT}{q} \left(\ln\left(J_{sc}\right) - \ln\left(J_0\right)\right) \tag{2.3}$$

Here, n is the ideality factor of the solar cell, k_B is the Boltzmann constant, T is the temperature of the solar cell, q is the elementary charge, J_{sc} is the short circuit current density and J_0 is the saturation current density. Furthermore, the saturation current density is can be defined with equation 2.4.

$$J_0 = BT^{\gamma} exp\left(-\frac{E_g}{k_B T}\right) \tag{2.4}$$

B is a constant that is assumed to be temperature-independent [3], the factor γ encompasses all material-dependent temperature dependencies and E_g being the absorber material bandgap. Substituting equation 2.4 into equation 2.3 leads to the following.

$$V_{oc} \approx \frac{nk_B T}{q}\left(\ln(J_{sc}) - \ln\left(BT^{\gamma} exp\left(-\frac{E_g}{k_B T}\right)\right)\right) = \frac{nk_B T}{q}\left(\ln(J_{sc}) - \ln B - \gamma \ln T + -\frac{E_g}{k_B T}\right) \tag{2.5}$$

It is further assumed that in equation 2.5 hat both B and J_{sc} have negligible temperature dependence. Now, the temperature-coefficient for the open-circuit voltage can be calculated using equation 2.6.

$$\frac{\partial V_{oc}}{\partial T} = \frac{V_{oc}}{T} + \frac{nk_B T}{q}\left(-\frac{\gamma}{T} - \frac{E_g}{k_B T^2}\right) = -\left(\frac{nV_g - V_{oc}}{T} + \gamma\frac{nk_B}{q}\right), \text{ with } V_g = \frac{E_g}{q} \tag{2.6}$$

This coefficient is present in the data sheet of the manufacturer. It is always negative, implying that a higher module temperature will lead to a lower open-circuit voltage. This coefficient can be used to estimate the V_{oc} at varying temperatures using equation 2.7 [3].

$$V_{oc}(T_M, G_{STC}) = V_{oc}(STC) + \frac{\partial V_{oc}}{\partial T}(STC)(T_M - T_{STC}) \tag{2.7}$$

Where T_M is module temperature, G_{STC} is the standard test conditions irradiance of 1000 W/m^2 and T_{STC} is the module temperature at the standard test conditions temperature of 25°C.

2.3. Current Thermal Management Solutions for PV Modules

There are many technologies that aim to reduce the negative effects of temperature on photovoltaic modules. Improving module efficiency by reducing operation temperature is the main goal of these technologies. Many of these technologies rely on the transportation of heat through a medium, albeit a solid, liquid or a gas. Research is still being conducted in this field to further reduce these negative effects and improve the efficiency of current technologies. Some of these technologies will be presented in this subchapter.

2.3.1. Water Cooling Systems

Many photovoltaic thermal (PVT) collectors utilize liquids as a method of cooling down the system. One of the most common used media is water, which has a high heat transfer coefficient. Examples of active methods in this field are as followed.

- **Forced water circulation systems**. This active method utilizes pipes attached to the rear side of the module. By pumping water through these pipes, the water can take up heat from the solar module. This heat can then be used for other applications, which can increase the overall efficiency of the system. However, the effectiveness of this method relies on the heat transfer capacity of the pipes. Furthermore, high material and maintenance costs come with this technique and may not be a suitable solution for large solar plants [11].
- **Liquid immersion cooling systems**. For this method, solar modules are fully submersed in water. Water is then the surrounding medium and thus much more heat can be absorbed, keeping the operating temperature low. This technology does posses a high-temperature reduction potential, however this method is more easily applied to smaller solar modules seeing that less water is then needed [11].

- **Floating PV systems**. This method of thermal management places solar modules on top of large area water surfaces. The solar modules are installed close to the water surface, this will in turn effectively reduce ambient temperature around the solar module. However, in a study conducted by Ziar et al. [12], frame soaking of the floating PV modules had a very minor influence on module performance and does not bring added values. Furthermore, it was reported that inland water areas have low effective albedo (6.5%). This low albedo does not contribute to a higher energy yield and makes water less favorable for bifacial PV installations.

2.3.2. Phase Change Materials (PCM)

Phase Change Materials (PCM) absorb and release heat by means of going through their respective freezing and melting cycles [11]. This technology has been studied by TU Delft alumni M.P.F Verheijen and C. van Nierop y Sanchez together with researcher J.C. Ortiz-Lizcano [13]. Phase change materials store the heat generated by a PV module during operation as latent heat rather than sensible heat, allowing phase change to occur at constant temperature. This process is visualized graphically in figure 2.3.

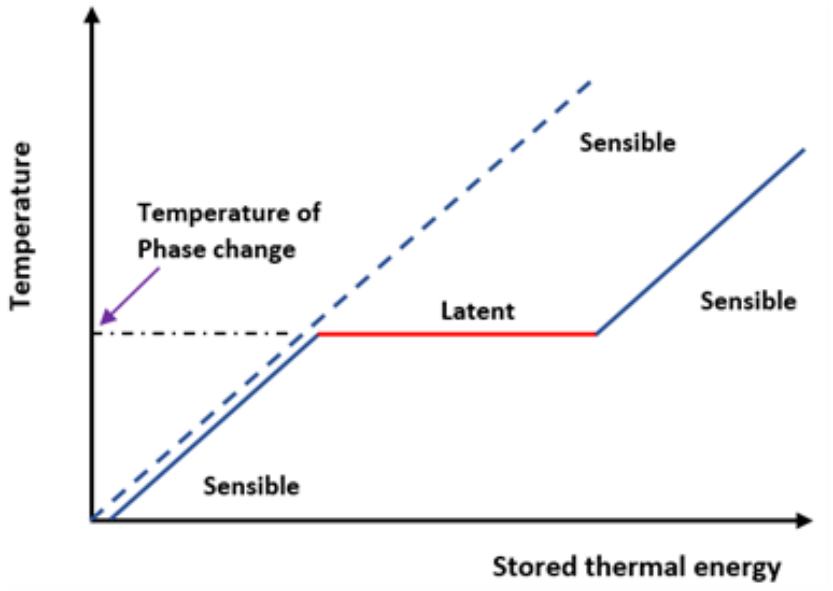

Figure 2.3: Schematic representation of latent heat storage in phase change materials. At the temperature of phase change, the material starts absorbing heat as latent heat rather than sensible heat [14].

These materials (e.g. organic oils or inorganic salt hydrates) have heat capacities several times larger than that of water or air. Also, the stored latent heat can be utilized for other purposes, for example water heating. This expands the purpose of the solar modules and can increase the overall efficiency of the system. This method falls under the passive cooling category, meaning that no electricity is consumed during operation and maintenance is minimal. An example of implementation can be seen in figure 2.4.

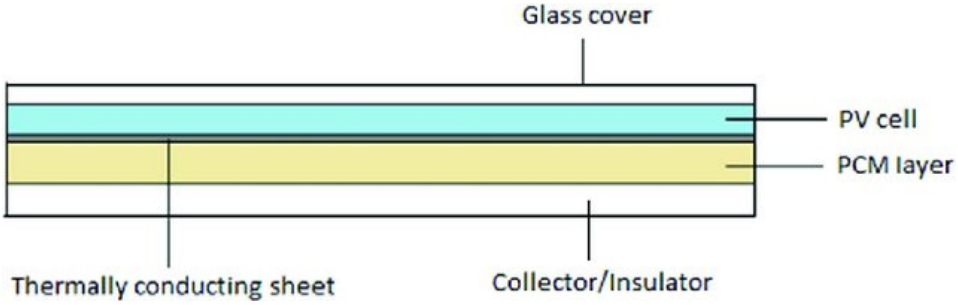

Figure 2.4: Integration of a PCM layer on the backside of a solar module [15].

2.3.3. Heat sinks

Heat sinks are commonly utilized in thermal management solutions for (monofacial) solar modules. This method relies on increasing the convective heat transfer of the solar module to the air by installing additional components to the back of the modules. The components can be for example microchannels or heat dissipating fins, which can be seen in figures 2.5 and 2.6.

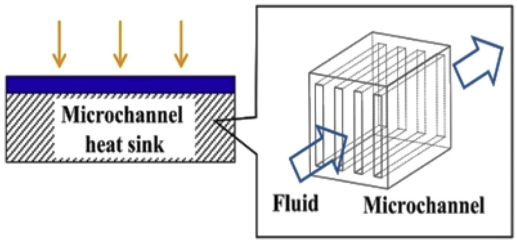

Figure 2.5: Schematic design of a microchannel structure attached to a PV module. Fluids are allowed to flow freely through the channels, allowing increased heat transfer to the environment [11].

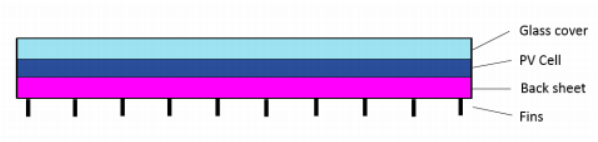

Figure 2.6: Heat dissipating fins design attached to the back of a PV module [16].

In a microchannel design (figure 2.5), a structure is installed at the back of a solar module that has many channels that run throughout the entire structure. By having many channels, the overall surface for heat transfer is increased and thus much more heat can be taken away from the module by the passing of a medium. The same principle is used for heat dissipating fins. Long, metallic fins increase the overall surface area for heat transfer, which can be seen in figure 2.6. Heat dissipating fins are a simple solution for PV thermal management. They require little to no maintenance and, being a passive solution, require no electricity to operate. Aluminum or copper are commonly used metals during manufacturing. These metals have a high heat transfer coefficient and are of low cost.
The effectiveness of heat sinks are dependent on ambient conditions during the operation of PV modules. Factors such as panel orientation and elevation, the geometry and design of the heat sink and wind speed presence are key elements in this technology. An example of a commercially available heat sink is the Coolback®, designed by the COOLBACK Company B.V. in Groningen, the Netherlands [17]. The Coolback® has a metallic, pyramidal structure that replaces the PV module frame, which can be seen in figure 2.7. This structure increase the heat transfer from the module to the environment, effectively increasing the energy output, reducing the operational temperature and prolonging the lifetime of the module.

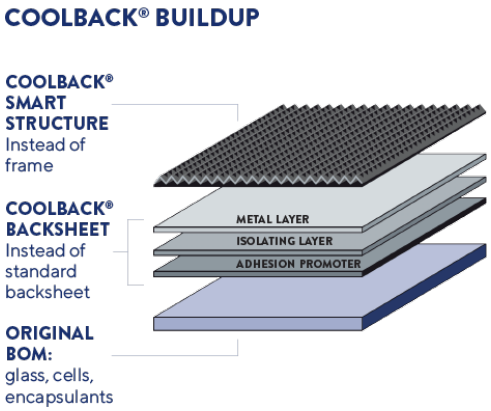

Figure 2.7: Schematic overview of the Coolback®. The structure is attached to the back of the module by an adhesion promoter as well as an isolating layer and a metal layer [17].

3

Simulation Model

In this chapter, the models created to study temperature effects on a bifacial solar module are described. To study the potential beneficial effects of an integrated heat sink (IHS), the program COMSOL Multiphysics 5.4 was used, alongside GenPro4, MATLAB and SAM. COMSOL is a software that allows the user to conduct multiphysics modeling. Based on finite element method (FEM) analysis, this software allows the user to generate or import any geometry, assign materials to each geometry and allows an easy integration of heat transfer mechanisms. This way, temperature variations along the geometry can be studied and analyzed. Furthermore, a description on how yield calculations were performed alongside lifetime prediction analyses are also presented.

3.1. Model geometry and materials

The size of the bifacial solar module was based on the LG NeON^{TM} 2 BiFacial LG300N1T-G4 module [18]. However, the data sheet for this module does not include information on the specific geometry and properties of the solar cells, these were obtained from other sources. This module has 60 solar cells, in arrays of 10. The dimensions for this module is 1640 x 1000 x 40 mm and each solar cell is 15.24 cm by 15.24 cm (6 inches by 6 inches). A schematic representation of the module, with and without the inclusion of the IHS, can be seen in figure 3.1a and figure 3.1b, respectively. The materials used for this module were glass, monocrystalline silicon, aluminum (IHS) and ethylene-vinyl acetate (EVA). EVA is a commonly used encapsulant material which is optically transparent and has a low thermal resistance. The IHS was placed between the bottom glass layer and the bottom EVA layer. This was done to electrically isolate the IHS from the PV layer, while still allowing heat transfer from the PV layer to the IHS to occur.

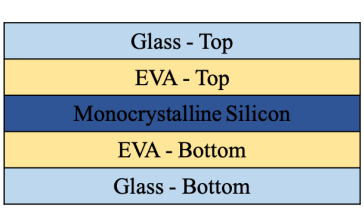

(a) Schematic representation of cell design.

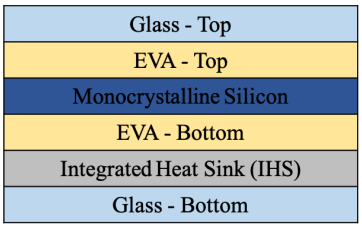

(b) Schematic representation of cell design including the IHS.

Figure 3.1: Schematic representation of cell design with and without the IHS.

Originally, the entire bifacial module was to be modeled in COMSOL. Since COMSOL supports imported computer-aided design (CAD) files, the necessary layers were drawn in the program AutoCAD and then imported in COMSOL. However, many problems arose during simulations, such as improper meshing and unrealistic results. It was then decided to create the geometry in the COMSOL environment and eventually scaling the module down to a single cell configuration. The main reason for this was to improve computation time. The module was first scaled back from a 6 by 10 to a 3 by 5 model. When the problems persisted, it was further scaled to a 2 by 1 design and then lastly to a single cell design (1 by 1).

Table 3.1: Dimensions of a single cell (1 cm by 1 cm) design.

Layer	Length and width (mm)	Thickness (mm)
Glass	11.67 x 11.67	3
Ethylene-vinyl acetate (EVA)	11.67 x 11.67	0.45
Monocrystalline silicon	10 x 10	0.18
Integrated heat sink (IHS)	Outer: 11.67 x 11.67 Inner: 10 x 10	1

It was noticed that even scaling the model down to a single cell, the built-in mesh settings that were used (which will be further explained in chapter 3.2.4) were leading to a very long computation time. It was then decided to perform two further adaptations to the model:

1. Further scaling down the model to where the dimension of the silicon layer is 1 cm by 1 cm. The length and width of remaining layers were then proportionally scaled down as well, while maintaining the same thickness . These final dimensions are summarized in table 3.1.

2. Adapting the mesh to a user-defined one to reduce computation time. After many helpful meetings with COMSOL employee Sander Bezuijen, a customized mesh was built, which is further explained in chapter 3.2.4. In order to build this mesh, each layer needed to be divided into two regions by means of extrusion.

    - The first extrusion has the top face of the silicon layer as the base and was extruded in the positive z-direction with a height of the EVA thickness and glass thickness (3.45 mm). This is valid for both models (with and without the IHS)
    - The second extrusion has the bottom face of the silicon layer as the base and was extruded in the negative z-direction with a height of the EVA thickness and glass thickness (3.45 mm). This was done for the model without the IHS. For the model with the IHS, the extrusion was performed with the IHS thickness included (4.45 mm).

Each layer remains one single, whole geometry and will physically simulate as such. However, now with two domains within the geometry, different mesh types and sizes can be assigned that can greatly reduce computation time. This will be further explained in chapter 3.2.4.
To further aid the computation time, a straightforward design was made for the bifacial solar cell by mirroring a monofacial cell.
In COMSOL, the user can assign a correspondent material for each layer. Other parameters that are needed for the simulation can also be found in the material assignment window. COMSOL has an extensive material library which was used for this model. The materials used are summarized in table 3.2.

Table 3.2: Layer thicknesses and assigned materials.

Layer	Assigned Material from COMSOL Library
Glass	Glass (Quartz)
Ethylene-vinyl acetate (EVA)	Elvax 250 (28% VA, 25 MI)
Monocrystalline silicon	Silicon
Integrated heat sink	Aluminium

3.2. COMSOL Multiphysics definition

To study the effect of heat on this bifacial module, with and without the IHS, two heat studies were coupled in COMSOL. These studies were 'Heat Transfer in Solids' and 'Surface-to-Surface Radiation' and together they form the interface 'Heat Transfer with Surface-to-Surface Radiation'. These two studies encompass the three basic heat transfer mechanisms, which are conduction, convection and radiation [3]. How COMSOL utilizes these three mechanisms are as follows.

- **Conduction**
  Conduction is the transfer of heat in a medium due to the presence of a temperature gradient. In COMSOL, this heat transfer can be either constant or temperature dependent. This is mathematically defined by Fourier law, which is shown in equation 3.1.

$$q = -\kappa \Delta T \tag{3.1}$$

  Here is q the heat flux density in W/m^2, κ the thermal conductivity in W/mK and ΔT the temperature gradient in K/m.

- **Convection**
  In this second heat transfer mechanism, convection is the transfer of hereby the movement of a fluid medium. In COMSOL, this can modeled for both free and forced convection as well as for laminar and turbulent flows. Convection is further calculated using Newton's law, which is shown in equation 3.2.

$$\dot{q} = -h(T_m - T_\infty) \tag{3.2}$$

  Here, $\dot{q}$ is the convective heat flux in W/m^2, h is the heat transfer coefficient in W/m^{2}K, which can be calculated by the program or be defined by the user, T_m is the module temperature and T_∞ is the temperature of the medium away from the module.

- **Radiation**
  The third heat transfer mechanism is radiation. This form of heat transfer is emitted by objects (depending on their temperature) and is a result of excited electrons falling back to their initial states, thereby emitting electromagnetic radiation [3]. This is represented in COMSOL by 'Surface-to-Surface Radiation', 'Surface-to-Ambient Radiation' and 'External Radiation'. The total heat emitted by a blackbody can be calculated using the Stefan-Boltzmann law, as shown in equation 3.3.

$$M_e = \epsilon \sigma T_s^4 \tag{3.3}$$

  Here is M_e the radiant emmitance in W/m^2, σ the surface emmisivity, σ the Stefan-Boltzmann constant and T_s is the surface temperature in Kelvin (K).

3.2.1. Heat Transfer in Solids

As mentioned before, the 'Heat Transfer in Solids' study handles all conductive and convective heat transfers. The settings that were used during simulations are presented below.

Solid 1

This node includes all domain selections and model inputs. Standard settings were used. The volume reference temperature T_{ref} was set to 'Common model input' and coordinate system was set to 'Global coordinate system'. The three parameters required to use this study, which are thermal conductivity (κ), material density (ρ) and the heat capacity at constant pressure (C_p) were all taken from the material assigned from the database. However, when assigning the materials to layers, COMSOL assigns values for thermal parameters. Many of these have been adapted and are summarized in table 3.3.

Table 3.3: Thermal parameters values used for each material during modeling.

Material	Density [kg/m^3][19]	Thermal conductivity [W/mK][19]	Heat capacity (C_p) [J/kgK][19]	Emmisivity (ε) [-]
Glass (Quartz)	2700	1.8	750	0.853 [20]
EVA - Elvax 250 (28% VA, 25 MI	960	0.32	2090	0.8 [21]
Silicon	2300	149	838	0.9 [22]
Aluminum	2700	238	900	0.09 [23]

Initial Values 1
This node assigns initial values to the entire domain. The initial temperature was set to the COMSOL standard of 293.15 K.

Thermal Insulation 1
This node is set to cover the entire geometry by default. This boundary condition means that there is no heat flux across the boundary and specifies that the domain is well insulated [24].

3.2.2. Calculation of heat transfer coefficients
To properly simulate the flow of heat in the solar module, heat transfer coefficient were calculated. This was calculated for the top and bottom glass layers using a MATLAB code, developed by PVMD colleague Andres Calcabrini, based on the Fuentes model [25]. After selecting 'Solid' material, selecting 'Convective heat flux' and selecting a 'User-defined heat transfer coefficient', one can assign the calculated heat transfer coefficient to the desired boundary. The heat transfer coefficients for the bottom glass layer and top glass layer were calculated to be 3.7022 W/m^{2}K and 4.7249 W/m^{2}K, respectively. Ambient temperature was set to 25°C and the irradiance to 1000 W/m^2 to mimic standard test conditions. Other ambient properties were set to ambient conditions of Delft on the 2nd of August, 2020 using the Dutch PV Portal [26]. These values for the heat transfer coefficients were then treated as a given and set for all simulations. Finally, the 'External temperature' was selected to be 'User defined' and set to 293.15 K.

3.2.3. Surface-to-Surface Radiation
This study handles all radiative heat transfer in a heat transfer simulation. The settings used for the performed simulations are as follows.

Diffuse Surface 1
Diffuse surfaces reflect radiative intensity uniformly in all directions. This is the default setting in the node for the entire geometry [24]. One important aspect in this study is the radiation direction. Firstly, in the general settings of the study, the 'Wavelength dependence of surface properties' is set to 'Constant'. Then, the 'Radiation direction' in this subnode is set to its default 'Opacity controlled'. In the following subnode 'Ambient', the ambient temperature is set to 'User defined' and to 293.15 K; the diffuse irradiance is set to 'User defined' and to 0 W/m^2.

Initial Values 1
In this subnode, an initial temperature is set to the entire geometry. The default 'Blackbody/Graybody' setting is selected with an initial value of 293.15 K.

Added node - Opacity 1 - Opaque Geometry
After receiving some errors during simulations, the following setting was added. After choosing the 'Opacity' option in the 'Surface-to-Surface' study, the entire geometry was selected and set to 'Opaque'.

Added node - Opacity 2 - Transparent Void
Coincidentally, to ensure that the space surrounding the solar cell is entirely transparent and does not interfere with heat transfers in the opaque geometry, a node was added by first selecting 'Opacity'. In the boundary selection, 'Infinite Void' was selected and set to 'Transparent'.

Added node - External Radiation Source 1

To simulate standard test conditions, an external radiation source of 1000 W/m^2 was added. This source was positioned at an 'Infinite distance' from the geometry and was directed in the negative z-direction with a normal vector **i**= (0,0,-1).

Added node - External Radiation Source 2

Since the solar module is bifacial, a second external radiation source is needed to simulate radiation coming from the positive z-direction, with normal vector **i**=(0,0,1). One more source was positioned at an 'Infinite distance' from the geometry and four values were simulated: 50 W/m^2, 100 W/m^2, 200 W/m^2 and 300 W/m^2 [27].

3.2.4. Mesh

In order for COMSOL to perform simulations, a mesh that encompasses the entire geometry is needed. Meshes divide the geometry into smaller, general areas that will be solved locally to obtain a global result. The size and type of mesh is defined by the user and will result in a finite number of elements that have a big impact on computation time.
Firstly, the size of the mesh was set to a COMSOL predefined setting of 'Normal'. Next, as previously mentioned, Sander Bezuijen of COMSOL NL devised a custom mesh that required the geometry to be divided in two domains purely for meshing purposes. Ultimately, what is a called a mapped mesh and a swept mesh was created.

Mapped mesh

The first domain encompassed the two extrusion that were created that run throughout the entire model. To facilitate the square geometry, a mapped mesh was assigned to this domain by selecting each section of each layer that falls into this new domain. Once this selection was completed, a new distribution was added into this section of the mesh. This new 'Distribution 1' has the same selection as the previous, but here the user can assign the number of elements that will be applied to each layer. The elements were rectangular in order to better accommodate the geometry. After investigating through trial-and-error, it was decided to assign 6 elements to this distribution as this is around the computation limit of the server used. This comes to a total of 36 elements in each face of this domain. This section of the mesh can be seen in figure 3.2.

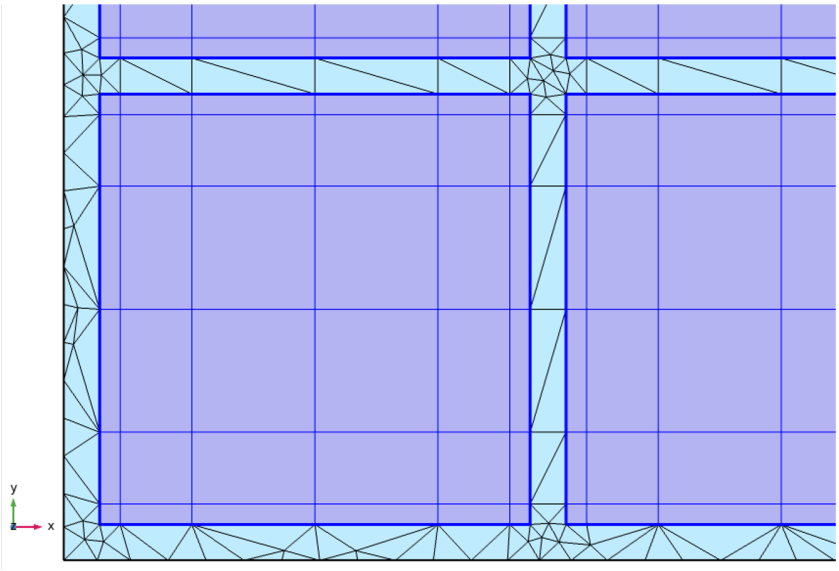

Figure 3.2: Orthogonal view of mapped mesh. This mesh consists of rectangular elements and is highlighted with purple.

Swept mesh

The second domain was meshed using a swept mesh, which can be seen in figure 3.3 and figure 3.4.

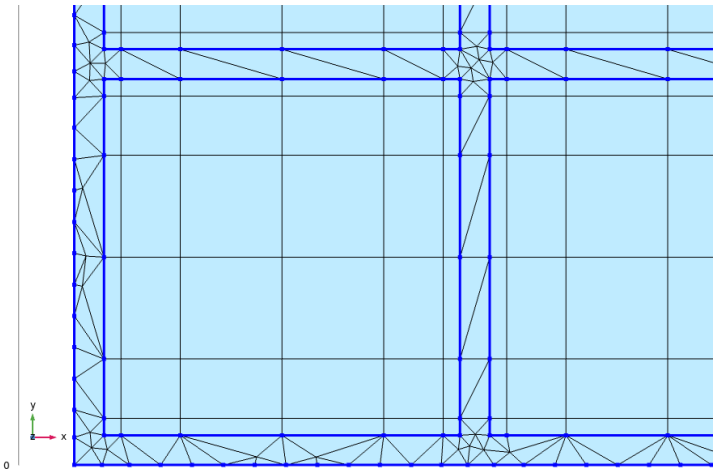

Figure 3.3: Orthogonal view of section of the swept mesh. This mesh consists of free tetrahedral elements and is contained within the highlighted dark blue lines.

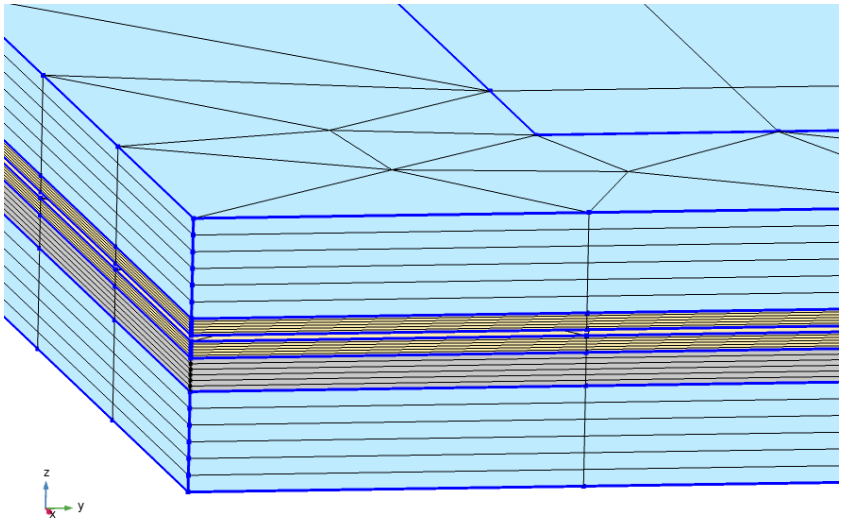

Figure 3.4: Side view of the swept mesh, consisting of six elements for each section of each layer. It was decided to assign six elements to facilitate computation time.

This mesh was applied for the remainder of the geometry. A distribution was also added to assign the number of elements to divide the side of the geometry. For this 'Distribution 1' the number of elements was also set to 6 to facilitate computation time. This 'hybrid' mesh effectively reduced the number of elements and the computation time, allowing the simulation to run and be completed. When testing new methods, results could have been quickly obtained and any problems encountered in the model could have been quickly debugged.

3.2.5. Geometry boundaries

When assigning materials to layers in COMSOL, these are generally assigned to the domains. However, boundaries also need to be assigned materials, especially when using the 'Surface-to-Surface Radiation' node. COMSOL prompts the user to do this and assign a surface emmisivity value to these boundaries. Boundary selection can be a tedious process, especially when the geometry in question is very large. The best way to perform this is to assign an 'Explicit' selection in the 'Definition' node.

For each layer, the domain must be selected and saved. In the same node, an 'Adjacent' selection is assigned to a layer and both the 'Exterior' and 'Interior' boundaries must be included. This process is repeated for each layer and then all boundaries are grouped. To assign the necessary surface emmisivity values, a blank material is created in the 'Materials' node. For each new grouped boundary the surface emmisivity value can now be assigned and controlled.

3.3. Yield calculations

To receive further insight in the effectiveness of the IHS and the possible energy benefits, yield calculations were performed.
Firstly, a location was needed. Alice Springs in Australia was chosen for its low diffuse to global irradiation (D2G) coefficient, which is 0.26 [28]. The optimal angle for this location is a 26° tilt facing north. This data was also used to calculate the plane of array (POA) irradiance for the PV module in the program SAM (v. 2021).

Next , it should be noted that since this is a bifacial module, the rear irradiation was also calculated. This was done at height of 1 meter from ground from the center of the module. The method used to calculate bifacial irradiation was based on a study by Pelaez et al.[29].

Furthermore, it was assumed that the summation of the front and back irradiance equals the total POA irradiance. A GenPro4 [30] simulation was performed to calculate the transmissivity value of layers encapsulating the PV layer. The cell designs of figure 3.1 were used and a transmissivity value of 0.93 was obtained. It was then assumed that the irradiance that reaches the PV layer is 0.93 times the POA irradiance. Using the ambient data from the program Meteonorm as input data for COMSOL, the average temperature of the PV layer could be calculated for both a module with and without the IHS. A 2 by 2 (34.29 cm by 34.29 cm) module was chosen to facilitate computation time and the following assumptions were made for the COMSOL simulations.

- The four months with the highest irradiation were selected based on Meteonorm data. This was done to facilitate computation time and the months selected were January, February, March and April.
- To further facilitate computation time, 12 hours were simulated to represent 1 day of irradiation, from 06:30 to 18:30.

These results for the average temperature were then used as input in a MATLAB code. Thermal data from a study by Yang et al. [31] was also utilized. With this code, the energy production in kWh/m^2 was calculated per month.

3.4. Lifetime prediction analyses

Lifetime prediction analyses were performed to calculate the difference in module lifetime with and without the IHS. These analyses were based on a study by Kaaya et al. [32]. These calculations were performed in MATLAB, the code of which can be found in Appendix B.2. In the study by Kaaya et al. [32], three degradation precursor reactions were considered that will lead to module degradation over time. These three parameters were:

- Hydrolysis-driven degradation due to temperature and relative humidity (k_H)
- Photodegradation due to UV dose, temperature, and relative humidity (k_P)
- Thermomechanical degradation due to temperature cycles (k_{Tm})

A majority of the datasets used for the calculation of these parameters were location-dependent data found during the study. Three locations were studied in this paper and it was decided to take k_H and k_P values of the warmest location (Negev) to facilitate calculations. The k_{Tm} value was to be calculated using equation 3.4 and using values obtained during the yield calculations.

$$k_{Tm} = A_{Tm}(\Delta T)^{\theta} C_n exp\left(-\frac{E_{Tm}}{k_B T_U}\right) \tag{3.4}$$

where

- A_{Tm}, pre-exponential constant [32],
- ΔT, temperature difference between the highest and lowest measured temperature of the module during operation,
- θ, model parameter that indicates the thermomechanical impact on power degradation [32],
- C_n, cycling rate [32],
- E_{Tm}, activation energy of power degradation [32],
- k_B, Bolztmann constant,
- T_U, upper (maximum) temperature of the PV module during operation.

The values used for the calculation of k_{Tm} are summarized in table 3.4. ΔT and T_U were assigned values from the warmest month during yield calculations, which was February.

Table 3.4: Parameter values used in equation 3.4

Parameter	**Value**
A_{Tm}	2.04 [-],
ΔT_{noIHS}	53.13 [K]
ΔT_{IHS}	53.02 [K]
θ	2.24 [-]
C_n	84.09 [-]
E_{Tm}	0.43 [eV]
k_B	$8.62{\cdot}10^{-5}$ [eV/K]
$T_{U,noIHS}$	348.62 [K], 75.47[°C]
$T_{U,IHS}$	348.51 [K], 75.36[°C]

The failure time can also be calculated using equation 3.5 and equation 3.6. The failure time was defined as the time it takes to module to lose 20% of its maximum power output [32].

$$t_f = \frac{B}{k_T \left(|log(0.2)|\right)^{\frac{1}{\mu}}} \tag{3.5}$$

$$k_T = A_N(1 + k_H)(1 + k_P)(1 + k_{TM}) + 1 \tag{3.6}$$

Here, t_f is the failure time in years, μ is the shape parameter and B is a model parameter, also known as power susceptibility. Also, k_T is the total degradation rate in %/year and A_N is the normalization constant of physical quantities in year^{-2}/%. The shape parameter μ was assigned a value of 0.19, the model parameter B was assigned a value of 190 and A_N was assigned a value of 1 [32].

4

Results and Discussion

In the following subchapters, temperature simulation results, yield calculations results and life cycle analyses results will be presented. This chapters consists of four sections:

1. Temperature simulations with and without the inclusion of the IHS in the PV module. Two module sizes were extensively studied: the 1 cm by 1 cm solar module and the 4 by 4 (67.31 cm by 67.31 cm) module. Two other module sizes were studied for comparison and sanity checks, which were the 2 by 2 (34.29 cm by 34.29 cm) module and the 3 by 3 (50.8 cm by 50.8 cm) module. The visual results of these last two modules can be found in Appendix A.1 and Appendix A.2.

2. Temperature simulations for varying IHS thickness. There were conducted with the 2 by 2 module to facilitate computation time.

3. Yield calculations. These were done by using a 2 by 2 module for simulations. Meteonorm ambient data was retrieved to calculate the PV layer temperature in COMSOL together with SAM and GenPro4. These values were then used as input data in MATLAB to calculate the yield for both modules so a comparative conclusion could be reached.

4. Lifetime prediction analyses results.

All results from the COMSOL simulations are stationary results with an ambient temperature of 20°C. For the 1 cm by 1 cm solar module and for the 4 by 4 module the front irradiance was set to 1000 W/m^2. For the back irradiance four values were simulated: 50 W/m^2, 100 W/m^2, 200 W/m^2 and 300 W/m^2 [27]. The visual results in the coming subchapters are for a front irradiance of 1000 W/m^2 and a back irradiance of 300 W/m^2. The remaining results are summarized in table 4.1 and table 4.2. For each results, the temperature difference for the PV layer was calculated. Then, the relative efficiency gain was calculated using the temperature coefficient of the reference module, which is -0.39%/°C [18].

4.1. 1 cm by 1 cm solar module

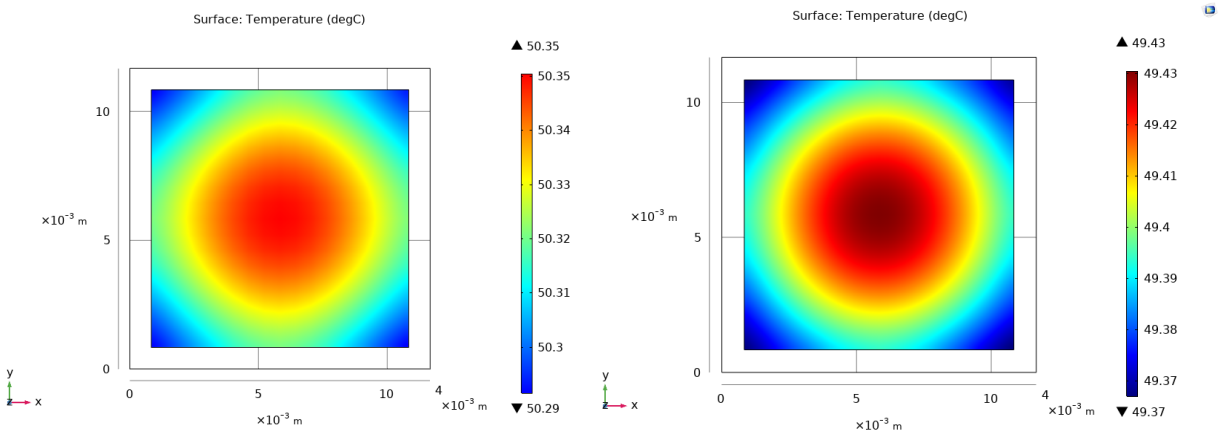

(a) without IHS

(b) with IHS

Figure 4.1: Temperature profile of 1 cm by 1 cm PV layer.

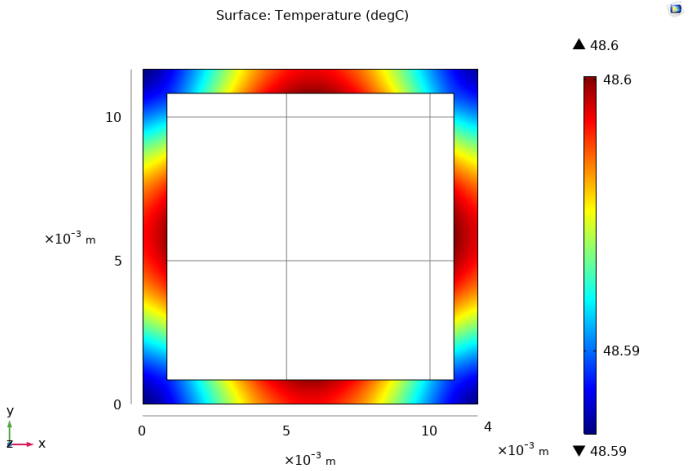

Figure 4.2: Temperature profile of the IHS in a 1 cm by 1 cm module.

The results for the 1 cm by 1 cm cell are shown in figure 4.1. In figure 4.1a the temperature profile of the PV layer can be observed without the IHS in the module. This configuration had a computation time of about 1 minute. It can be seen that the PV layer has an average temperature of 50.32°C. For the module configuration including the IHS, that can be seen in figure 4.1b, a similar temperature profile can be observed (this configuration had a computation time of 26 seconds). Also, a lower average temperature can be observed of 49.40°C. This resulted in an average temperature difference of -0.92°C and results in a relative efficiency gain of +0.359%.

It can be seen in the temperature profiles that the center of the PV layer is the hottest and the corners are the coldest, which is expected seeing that the irradiance from both the front and back side of the module are perpendicular to the geometry. The heat seems to be dissipating towards the middle of the edges of the geometry. This heat transfer profile can also be seen in the temperature profile of the IHS (figure 4.2). Even though the temperature across the IHS only differs with 0.01°C (comparing the coldest and hottest parts with each other), the difference is enough to visualize the corresponding heat profile and is in accordance with the profiles observed in the PV layers.

4.2. 4 by 4 solar module

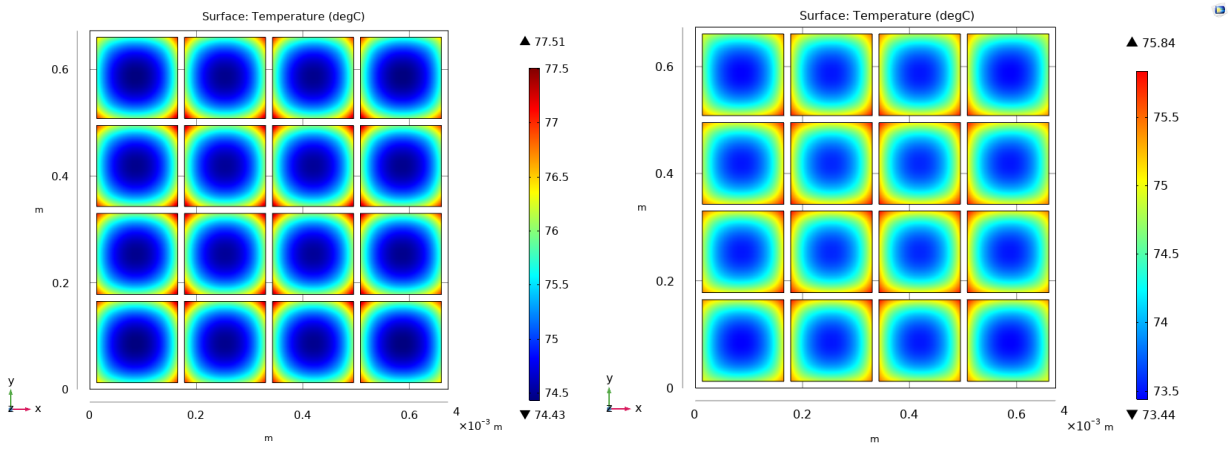

(a) without IHS

(b) with IHS

Figure 4.3: Temperature profile of the PV layer of a 4 by 4 module.

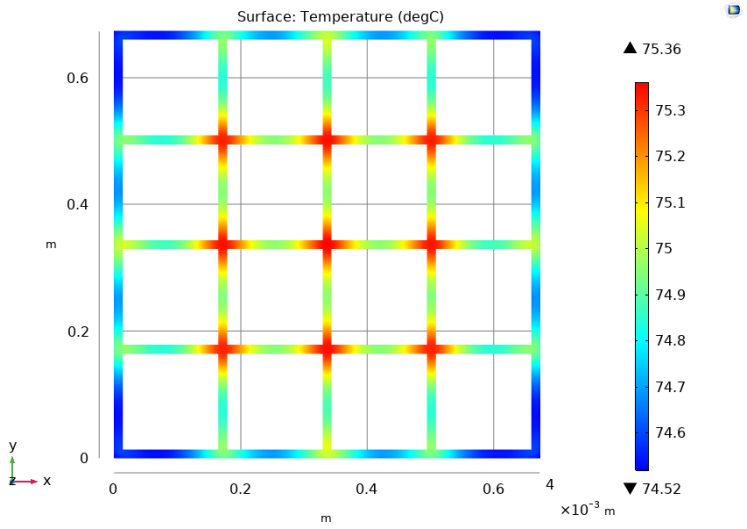

Figure 4.4: Temperature profile of the IHS in a 4 by 4 module.

After completing simulations on the 1 cm by 1 cm module, the module was scaled up to a 4 by 4 module and simulated under the same conditions. This resulted in an average computation time of 18 minutes. The temperature profiles for the PV layer with and without the IHS in the module can be seen in figure 4.3a and figure 4.3b, respectively. It can be observed that the average temperature of the PV layer without the IHS is 75.97°C. With the IHS this average temperature decreases to 74.64°C. This results in an average temperature difference of -1.33°C and a relative efficiency gain of +0.519%. In comparison to the 1 cm by 1 cm module, there is a significant rise in temperature. This can be attributed to way the model was scaled down, in which only the length and width were adjusted, but the thickness remained the same.
However, the temperature profiles of the 4 by 4 modules differs than that of the 1 cm by 1 cm modules, in that the centers of the PV cells are no longer the hottest parts. According to these results, the centers of the PV cells are the coldest parts of this layers and the corners of the cells are the hottest. If the entire module is taken into account, the four corners of the entire module are the coldest parts and the center of the module are the hottest parts. This 'mimics' the results of the 1 cm by 1 cm module and can be clearly seen in figure 4.4.

Upon further inspection, this central hotspots are attributed to the concentration of fine mesh elements in that area. To illustrate this, a zoomed in section of the 4 by 4 module can be seen in figure 4.5.
The corresponding mesh layer can be seen in figure 4.6.

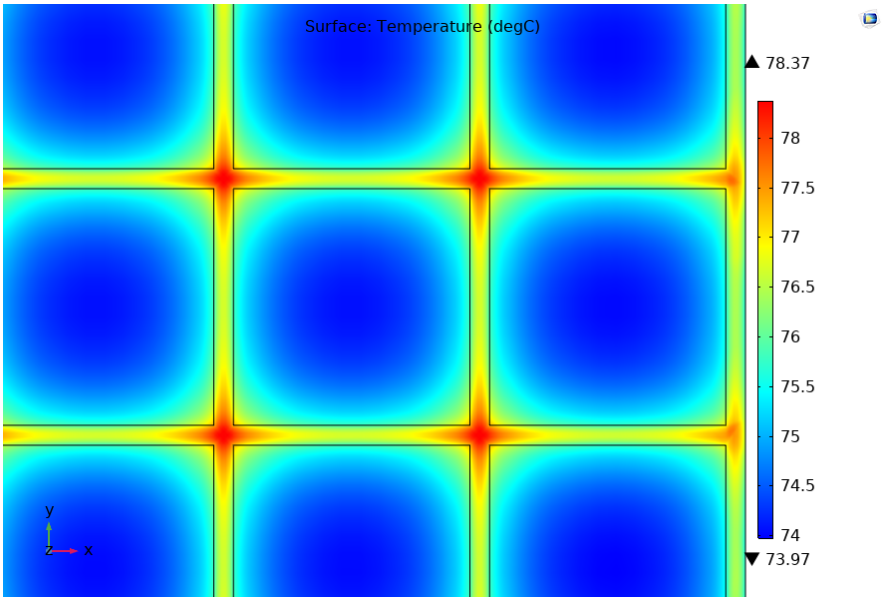

Figure 4.5: Zoomed in section of the 4 by 4 module temperature profile.

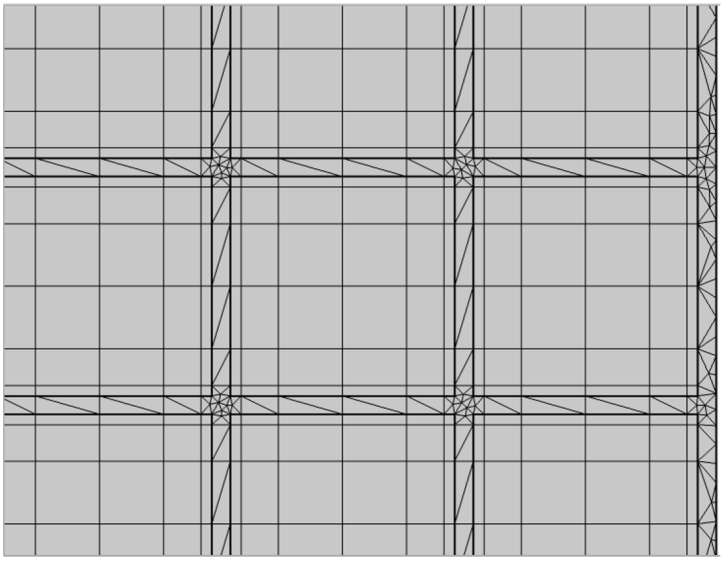

Figure 4.6: Corresponding mesh of zoomed in section of the 4 by 4 module temperature profile.

Fine and concentrated mesh elements can be seen at the center of four cells. During other simulations, no matter how coarse the inner, mapped mesh was made and due to the small geometry in that region, these hotspots were still being observed. In order to rule out other errors, a 2 by 2 module and a 3 by 3 module were constructed and simulated under the same conditions. However, the same temperature profile was observed and it became evident that this temperature profile was a result of the fine mesh concentration.

Table 4.1: PV layer temperature results from different simulation conditions. The displayed top bar are the values for the front and back irradiance.

		1000/50 W/m^2	**1000/100 W/m^2**	**1000/200 W/m^2**	**1000/300 W/m^2**
1x1	**no IHS**	44.71°C	45.85°C	48.11°C	50.32°C
	with IHS	44.01°C	45.11°C	47.27°C	49.40°C
2x2	**no IHS**	-	-	-	75.93°C
	with IHS	-	-	-	74.58°C
3x3	**no IHS**	-	-	-	75.94°C
	with IHS	-	-	-	74.60°C
4x4	**no IHS**	66.55°C	68.48°C	72.27°C	75.97°C
	with IHS	65.42°C	67.30°C	71.01°C	74.64°C

Table 4.2: Corresponding temperature difference and efficiency gain for modules with and without the IHS. The displayed top bar are the values for the front and back irradiance.

		1000/50 W/m^2	**1000/100 W/m^2**	**1000/200 W/m^2**	**1000/300 W/m^2**
1x1	**no IHS**	ΔT= -0.70°C	ΔT= -0.74°C	ΔT= -0.84°C	ΔT= -0.92°C
	with IHS	$\Delta\eta_{rel}$= +0.273%	$\Delta\eta_{rel}$= +0.289%	$\Delta\eta_{rel}$= +0.328%	$\Delta\eta_{rel}$= +0.359%
2x2	**no IHS**	-	-	-	ΔT= -1.35°C
	with IHS	-	-	-	$\Delta\eta_{rel}$= +0.529%
3x3	**no IHS**	-	-	-	ΔT= -1.34°C
	with IHS	-	-	-	$\Delta\eta_{rel}$= +0.523%
4x4	**no IHS**	ΔT= -1.13°C	ΔT= -1.18°C	ΔT= -1.26°C	ΔT= -1.33°C
	with IHS	$\Delta\eta_{rel}$= +0.441%	$\Delta\eta_{rel}$= +0.460%	$\Delta\eta_{rel}$= +0.491%	$\Delta\eta_{rel}$= +0.519%

A summary of all of the simulation results obtained can be seen in table 4.1 and in table 4.2. It can be noted that with increasing back irradiance the temperature of the PV layer increases accordingly. A temperature jump of at least 25°C can be observed between the 1 cm by 1 cm module and the other module configurations. Furthermore, for the highest irradiance combination there is a minimum relative efficiency gain of 0.359%.

4.3. Varying IHS thickness

To investigate the potential benefit of increasing the thickness of the IHS, seven different thickness values were simulated using the 4 by 4 module. The results of these simulations are summarized in table 4.3. This can also be seen graphically in figure 4.7 and figure 4.8.

Table 4.3: Temperature and efficiency change with varying IHS thickness.

IHS thickness (mm)	**PV layer temperature T$_{PV}$ (°C)**	**Temperature difference with IHS ΔT (°C)**	**Relative efficiency gain $\Delta\eta_{rel}$ (%)**
no IHS	75.97	-	-
1	74.64	-1.33	+0.519
2	74.59	-1.38	+0.538
3	74.58	-1.39	+0.542
4	74.57	-1.40	+0.546
5	74.55	-1.42	+0.554
7.5	74.51	-1.46	+0.569
10	74.43	-1.54	+0.601

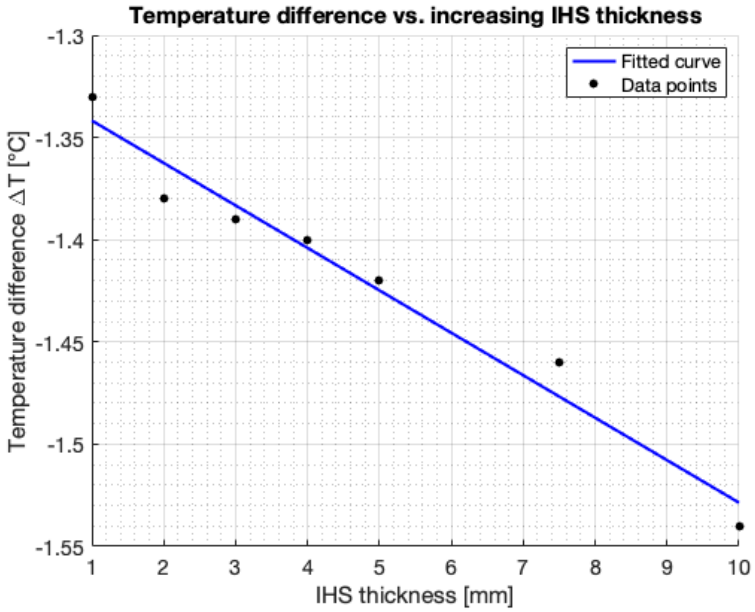

Figure 4.7: Temperature difference vs. increasing IHS thickness. Data points were fitted to obtain a temperature coefficient for increasing IHS thickness.

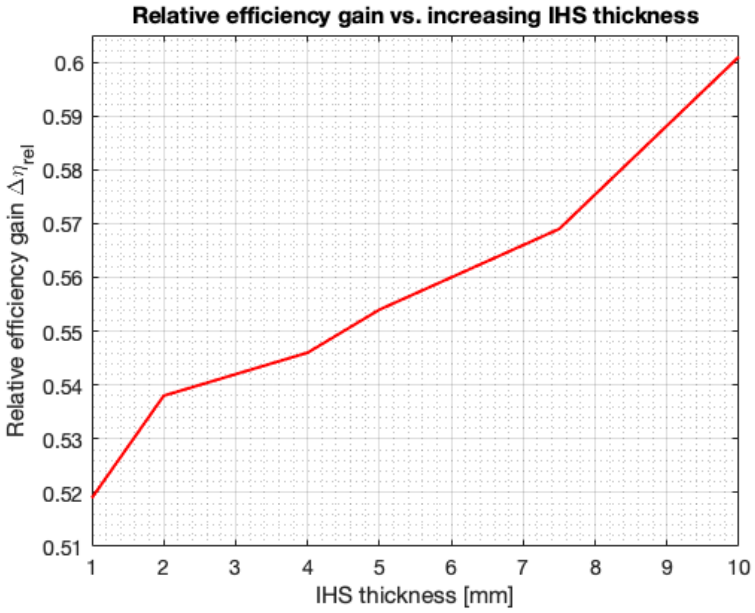

Figure 4.8: Relative efficiency gain vs. increasing IHS thickness.

A linear fit was applied to the data points in figure 4.7. The temperature coefficient was calculated to be -0.02076 °C/mm ± 0.00453 °C/mm. It should be noted however that this temperature coefficient is valid for a minimum IHS thickness of 1 mm. It was also found that for each increment of the thickness of the IHS, the relative efficiency gain also increases.
The initial temperature difference between a 1 mm IHS and no IHS is -1.33°C. By further increasing the thickness from 1 mm to 2 mm, the temperature difference decreases with only 0.05°C. When further increment is applied to achieve a 3 mm thickness, the temperature difference only decreases with 0.01°C.
Increasing the IHS thickness also has an influence in the overall weight of the module, which is summarized in table 4.4.

Table 4.4: Module weight difference with varying IHS thickness.

IHS thickness (mm)	Module weight (kg)	Weight difference compared to no IHS (kg)
no IHS	7.88	-
1	8.10	0.22
2	8.32	0.44
3	8.54	0.66
4	8.76	0.88
5	8.99	1.10
7.5	9.54	1.65
10	10.09	2.20

It can be noted that for every 1 mm of thickness added to the IHS, the total module weight increases with 0.22 kg. Furthermore, the module weight without the IHS is quite heavy (7.88 kg). This weight is attributed to the two glass layers that are present in module, which have a combined weight of 7.34 kg. With an IHS thickness of 5 mm, the total module weight will be increased with more than 1 kg. Comparing table 4.3 with table 4.4, it was decided to utilize an IHS thickness of 1 mm.

4.4. Yield calculations

As previously stated, the energy yield was calculated for modules with and without the IHS. First, the energy yield per m^2 (using the 2 by 2 module area of 0.118 m^2) for each month was calculated as well as the energy gain. The results for this calculation is summarized in table 4.5. Detailed results of each hour for each of the four months simulated can be found in Appendix C.

Table 4.5: Energy yield for each of the hottest months in Alice Springs, Australia. Results are for a 2 by 2 module, with and without the IHS.

Month	Energy yield without IHS (kWh/m^2)	Energy yield with IHS (kWh/m^2)
January	20.08	20.08
February	18.14	18.22
March	21.02	21.02
April	18.90	18.90
Total	**78.14 kWh/m^2**	**78.22 kWh/m^2**
Energy gain	**0.08 kWh/m^2**	

Now, the obtained values can be converted to a yearly basis by multiplying the results with a factor 3. The energy can then be compared to the price per kWh in Australia, which was 0.206 €/kWh (0.338 A$/kWh) in June 2020 [33]. The yearly energy yield and financial gain are summarized in table 4.6.

Table 4.6: Yearly energy yield and financial gain in Alice Springs, Australia. Results are for a 2 by 2 module, with and without the IHS.

Yearly energy yield, without IHS	234.43 kWh/m^2/year
Yearly energy yield, with IHS	234.66 kWh/m^2/year
Yearly energy gain	0.23 kWh/m^2/year
Financial gain	0.05 €/m^2/year

A financial gain of 0.05 €/m^2/year was found with the yield calculation. This number is low, however upon further inspection, this can be attributed to two main factors:

- Firstly, the IHS was placed between two layers: a 3 mm glass layer and a 0.45 mm EVA layer. This bottom glass layer hinders the heat transfer from the IHS to the environment. This can be improved by either making the bottom glass layer thinner or changing the material from glass to a transparent back layer.
- Secondly, the IHS does indeed take up thermal energy, but in this model no additional heat transfer mechanisms were designed. This leads to heat transfer mainly through the bottom glass layer. To increase this heat transfer, the integrated heat sink can be connected to the frame by metal contacts, therefore increasing the heat transfer area. This area can be further increased by the addition of heat dissipating fins possibly attached to the frame of the module.

4.5. Lifetime prediction analyses

As described in chapter 3.4, equations 3.4, 3.5 and 3.6 were used to predict the lifetime of a PV module with and without the inclusion of the IHS. The results of the total degradation per year k_T as well as the failure time t_f is summarized in table 4.7.

Table 4.7: Lifetime prediction results for a PV module with and without the inclusion of the IHS.

	k_H **[%/years]**	k_P**[%/years]**	k_{Tm}**[%/years]**	k_T**[%/years]**	t_f**[years]**
without IHS	0.169	0.216	0.7670	1.5119	10.27
with IHS	0.169	0.216	0.7601	1.5019	10.34
				Δt_f	+0.07

It can be seen that with the inclusion of the IHS, the lifetime gain is 0.07 years (0.68%), which is about 26 days. Another interesting result can be observed in table 4.7, which is the lifetime of the modules. The lifetime of the LG NeON^{TM} 2 BiFacial LG300N1T-G4 module is reported to be 25 years [18]. Here we can see that the lifetime of a module without the IHS is 10.27, which is significantly less than current reported lifetimes. This difference is due to the high maximum temperature that the module reaches (75.47 °C without IHS, 75.36 °C with IHS) as well as the large difference between the maximum and minimum module temperatures. It should be noted that ambient temperatures have an effect on the lifetime of a module, longer lifetimes are reported for colder climates [32].
As previously stated, these results depend heavily on location-dependent data. For example, the two parameters k_H and k_P require data such as relative humidity and the received UV dose, both of which are location-dependent. To improve this lifetime prediction analysis, these values should be measured of the location for which this analysis is conducted. Nonetheless, the importance of thermal management are now more evident. Increased temperatures do not only have a negative impact on the temperature of the module, it also has a great impact on the lifetime. This large decrease in lifetime is detrimental to PV projects of any scale as well as the investments necessary to build and maintain such projects.

5

Conclusion, Recommendations and Outlook

5.1. Conclusion

In this thesis, a passive cooling method has been presented to reduce the operational temperature of bifacial PV modules. This method relies on the inclusion of an integrated heat sink (IHS) between the bottom glass layer and the bottom EVA layer. This was to electrically isolate the IHS from the PV layer, while still allowing heat transfer from the PV layer to the IHS to occur.

Most passive cooling technologies are applied to monofacial modules. The focus of this study was to research the effect of the IHS in a bifacial module. To accomplish this, thermal models were developed in COMSOL Multiphysics 5.4. The use of this software enabled in-depth, thermal simulations for a bifacial PV module while controlling parameters such as heat transfer coefficients, front and back irradiance and ambient temperatures. After debugging meshing and geometry errors, simulations could be performed for various modules sizes (1 cm by 1 cm, 2 by 2, 3 by 3 and 4 by 4 modules), front and back irradiance values and ambient temperature values.

It was found that for the highest irradiance combination (front irradiance of 1000 W/m^2 and back irradiance of 300 W/m^2) the 1 cm by 1 cm module showed, with the inclusion of the IHS, an operational temperature reduction of 0.92°C. This corresponded with a relative efficiency gain of 0.359%. For the 4 by 4 module under the same conditions, a temperature reduction of 1.33°C was found as well as a relative efficiency gain of 0.519%. Further simulations were performed for increased thicknesses of the IHS. For a 4 by 4 module, an initial temperature reduction of 1.33°C was observed for a 1 mm thick IHS. Further increasing the IHS did not show significant temperature reduction, this also led to an overall weight increase of the PV module.

Yield calculations and lifetime prediction analyses were performed. For ambient properties of Alice Springs, Australia, the financial gain of the inclusion of the IHS was 0.05€/m^2/year. The lifetime of a PV module with and without the IHS was also predicted. It was found that the lifetime gain for a module with the IHS is about 26 days, corresponding to a gain of 0.68%. It should be noted however, that the lifetime of a module without the IHS under the simulation conditions was 10.27 years, far below commercially reported lifetimes. This is due to a high maximum operational temperature and a large difference between the minimum and maximum operational temperature.

It is evident that this passive cooling method can indeed lower the operational temperature of a bifacial PV module. The necessity of thermal management is further illustrated by the results obtained from yield calculations and lifetime prediction analyses. Seeing that the thermal management field for bifacial modules is a relatively new field, further research will greatly benefit the bifacial PV market. This can effectively reduce their operating temperatures, increase their electrical efficiency and overall energy yield.

5.2. Recommendation and Outlook

During the research conducted in this thesis, a number of potential adaptations were discovered that could significantly improve simulations and their outcomes. Based on the results presented, the following adaptations to the models should be made and investigated.

Firstly, a method on how to increase the heat transfer from the IHS to the environment should be investigated. Currently, a 1 mm IHS is able to reduce the operating temperature of the PV layer by a maximum of 1.35°C. This reduction in temperature can further be increased by investigating different materials for the IHS or by potentially connecting the IHS to the frame of the module. This can increase the heat transfer area. Another possibility is to further add heat dissipating fins to the backside of the module, further increasing the convective heat transfer in the presence of wind.

Next, the thickness and material of the bottom most layer should be adapted. A 3 mm thick glass layer hinders the heat transfer of the IHS to the environment. A thinner, transparent backsheet might be more suitable for this model. However, it was noticed that when the bottom glass layer was removed from the model (leaving the IHS exposed to the environment), the simulation could not be completed since the mesh was now incomplete. This would require remeshing and debugging as well as new heat transfer coefficients for the now exposed IHS.
Currently, the heat transfer coefficients for the top and bottom glass layers as well as the ambient temperature were calculated and then set as fixed values throughout simulations. It is more accurate to calculate new coefficient values each time the irradiance values are changed in COMSOL.

Looking into the possibility of adding the solar spectrum as the irradiance source in COMSOL should also be considered. An irradiance source fixed to infinity was used in the model. Adding a solar spectrum will increase the accuracy of the results. However, the new presence of wavelength-dependent parameters in the module will occur and further research into obtaining the necessary values for these parameters is then needed.

Regarding the yield calculations, the methodology should be extended to include all months of the year. Furthermore, the recalculation of the heat transfer coefficients should also be included, however this may be very tedious. Using a 2 by 2 model, with a computation time of around 1 minute and 30 seconds, lead to a total simulation time of 2.4 hours (data processing excluded). Adding the recalculation of the heat transfer coefficients will increase the total simulation time significantly.

For the lifetime prediction analysis, it would be beneficial to gather location-based data to further improve the accuracy of the results. Many of the equation input data used was from a different location compared to the temperature values. If input data can be measured and processed for Delft, accurate results can be obtained for the lifetime prediction of a bifacial module and the effectiveness of the IHS can be more evident.

Other programs should be explored for the conducted temperature management research. COMSOL performs well in this field by allowing the user to completely customize the simulation settings, increasing the accuracy of the results. However, larger geometries lead to larger meshes with increased mesh elements if a certain degree of accuracy is desired. This leads to a long computation time and large memory usage. This can be addressed by reducing the amount and size of mesh elements, however, this may lead to less accurate results. A point will be reached during research where the user will need to find the proper balance of accuracy versus computation time with the available computation memory.

Lastly, the geographical effectiveness of the IHS should be investigated. Simulations should be conducted for varying (extreme) ambient conditions, e.g. cold climates versus hot climates and the influence of varying wind speeds. Furthermore, experimental temperature testing should be conducted using a prototype of the IHS implemented in a bifacial module.

A

Appendix A - Temperature profiles of varying module sizes

A.1. Temperature profile of 2 by 2 PV module

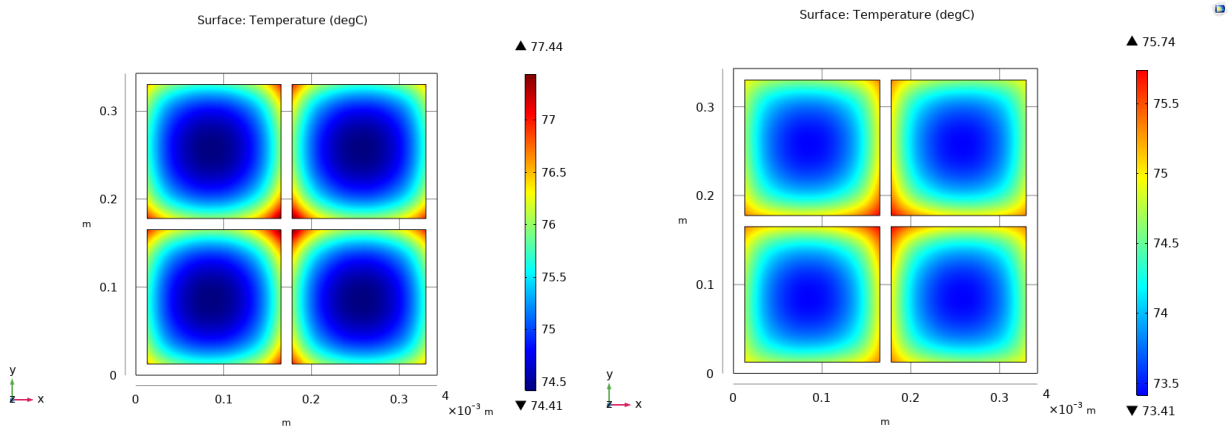

(a) without IHS

(b) with IHS

Figure A.1: Temperature profile of the PV layer of a 2 by 2 module.

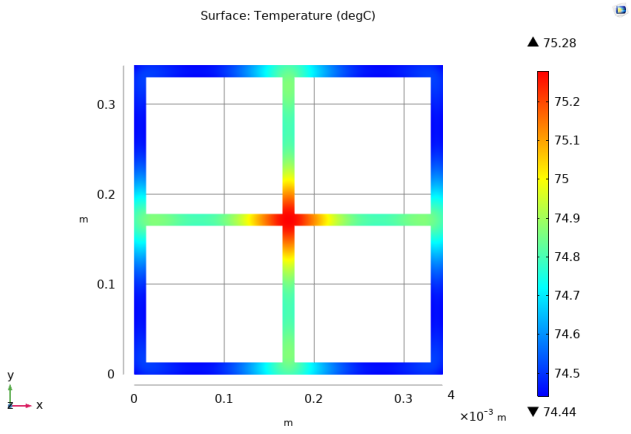

Figure A.2: Temperature profile of the IHS in a 2 by 2 module.

A.2. Temperature profile of 3 by 3 PV module

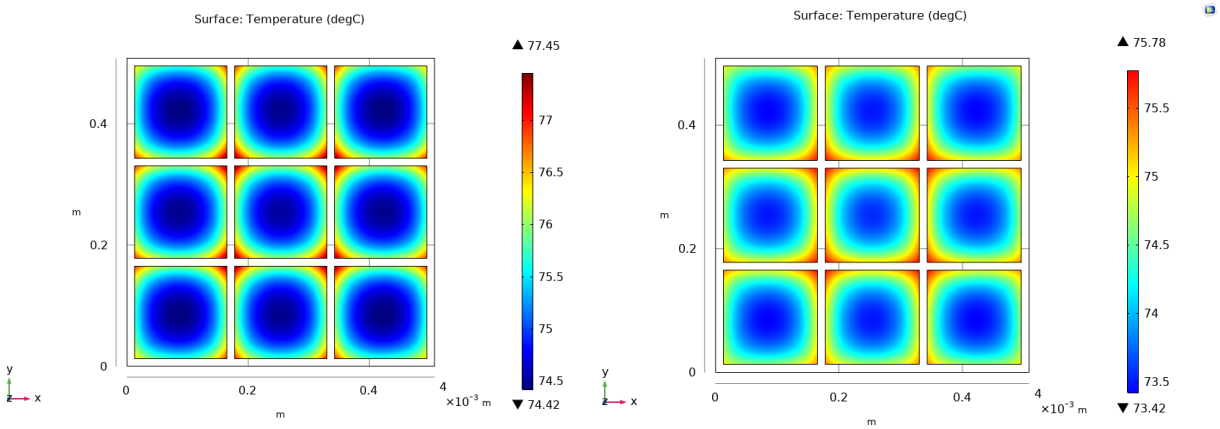

(a) without IHS

(b) with IHS

Figure A.3: Temperature profile of the PV layer of a 3 by 3 module.

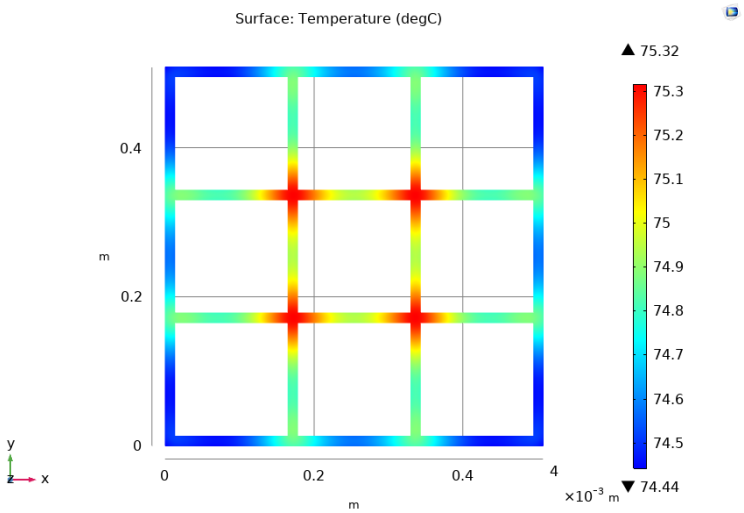

Figure A.4: Temperature profile of the IHS in a 3 by 3 module.

B

Appendix B - MATLAB codes

B.1. Yield calculation code

```
%% Yield calculations
%Author: Juan Camilo Ortiz-Lizcano
%%
load('GmL.mat');
load('TcL.mat');   %module temperature array without IHS
load('TchsL.mat'); %module temperature array with IHS

GmL2 = 0.93.*GmL;  %includes transmissivity
G_M_tot = GmL2(:);
Tm = TchsL(:);
%Solar cell data from Yang et. al
mpp_stc =3.4382;
voc_stc = 0.69144;
isc_stc = 6.5427;
impp_stc = 6.1335;
area_m = 155/10000;
kappa = -.39/100;

%%
eta_stc = mpp_stc/area_m/1000;
fill_factor = mpp_stc/voc_stc/isc_stc;
n_cell = 1;
ideality = 1.2;
voc_gm = voc_stc+n_cell*ideality*298.15*1.380649e-23/1.60217662e-19*log(G_M_tot/1000);
voc_gm(G_M_tot==0)=0;
isc_gm = isc_stc*G_M_tot/1000;
pmpp_gm = fill_factor*voc_gm.*isc_gm;
eta_gm = pmpp_gm./(G_M_tot*area_m);
eta_gm(G_M_tot==0)=0;

eta_real = eta_gm.*(1+kappa*(Tm-25));
mpp_real = eta_real.*G_M_tot*area_m;
pmpp_mat = reshape(mpp_real,size(GmL))*4 %times the number of cells
%%
jan = 31*sum(pmpp_mat(:,1))/1000; %[kWh]
feb = 28*sum(pmpp_mat(:,2))/1000; %[kWh/month]
mar = 31*sum(pmpp_mat(:,3))/1000; %[kwh/month]
apr = 30*sum(pmpp_mat(:,4))/1000; %[kWh/month]

totalmonths_kWh = jan+feb+mar+apr;
```

B.2. Lifetime prediction analyses code

```
%% Lifetime prediction analysis
%Author: Lyndon Wix
%Based on study conducted by Kaaya et al. 'Modeling Outdoor Service
%Lifetime Prediction of PV Modules: Effects of Combined Climatic Stressors
%on PV Module Power Degradation'
%%
clear all
close all

kh = 0.169; % %/year
kp = 0.216; % %/year

An     = 1;
Atm    = 2.04;    %pre-exponential constant
theta  = 2.24;    %thermo-mechanical model parameter
Cn     = 84.09;   %cycling rate
Etm    = 0.43;    %activation energy [eV]
kb     = 8.62E-5; %Boltzmann constant [eV/K]
B      = 190;     %model parameter (power susceptibility)
mu     = 0.19;    %shape parameter

Tu_noIHS = 75.47+273.15; %upper temperature in Kelvin no IHS
Tl_noIHS = 22.34+273.15; %lower temperature in Kelvin no IHS
Tu_IHS   = 75.36+273.15; %upper temperature in Kelvin IHS
Tl_IHS   = 22.34+273.15; %lower temperature in Kelvin IHS
dT_noIHS = Tu_noIHS-Tl_noIHS;
dT_IHS   = Tu_IHS-Tl_IHS;

ktm_noIHS = Atm*(dT_noIHS^theta)*Cn*exp(-Etm/(kb*Tu_noIHS));
kT_noIHS  = (An*(1+kh)*(1+kp)*(1+ktm_noIHS))-1; % %/year total
tf_noIHS  = B/(kT_noIHS*(abs(log(0.2))^(1/mu))); %years

ktm_IHS = Atm*(dT_IHS^theta)*exp(-Etm/(kb*Tu_IHS))*Cn;
kT_IHS  = An*(1+kh)*(1+kp)*(1+ktm_IHS)-1; % %/year total
tf_IHS  = B/(kT_IHS*(abs(log(0.2))^(1/mu))); %years

years_gained = tf_IHS-tf_noIHS;
days_gained  = years_gained*365;
```

C

Appendix C - Temperature results used for yield calculations

Table C.1: Temperature results of PV layer in °C used for yield calcuations. Twelve hours were simulated for each of the four months with and without the IHS. The ambient data of Alice Springs, Australia was used during simulations

		January (°C)	**February (°C)**	**March (°C)**	**April (°C)**
06:30	**no IHS**	25.51	22.34	19.11	14.25
	with IHS	25.50	22.34	19.12	14.25
07:30	**no IHS**	33.03	28.62	25.88	21.45
	with IHS	33.01	28.61	25.87	21.44
08:30	**no IHS**	45.14	40.96	39.51	33.83
	with IHS	45.09	40.92	39.47	33.79
09:30	**no IHS**	57.15	52.67	52.25	45.68
	with IHS	57.07	52.60	52.17	45.61
10:30	**no IHS**	67.27	63.60	62.44	55.74
	with IHS	67.17	63.51	62.35	55.65
11:30	**no IHS**	70.73	68.69	69.00	63.36
	with IHS	70.64	68.60	68.89	63.26
12:30	**no IHS**	74.01	73.94	73.30	67.14
	with IHS	73.91	73.84	73.20	67.03
13:30	**no IHS**	74.74	75.47	75.18	69.04
	with IHS	74.64	75.36	75.07	68.93
14:30	**no IHS**	73.01	72.01	72.02	66.8
	with IHS	72.91	71.91	71.92	66.7
15:30	**no IHS**	67.83	68.01	67.10	61.88
	with IHS	67.75	67.92	67.02	61.80
16:30	**no IHS**	60.79	60.56	58.95	51.89
	with IHS	60.72	60.49	58.88	51.82
17:30	**no IHS**	51.48	50.30	47.11	38.72
	with IHS	51.43	50.26	47.07	38.69
18:30	**no IHS**	40.67	38.33	30.42	25.18
	with IHS	40.65	38.31	30.42	25.19

Bibliography

[1] Max Roser. Future population growth. *Our World in Data*, 2013. URL https://ourworldindata.org/future-population-growth.

[2] Berkeley Earth. Global temperature report for 2017. URL http://berkeleyearth.org/global-temperatures-2017/.

[3] Arno HM Smets, Klaus Jäger, Olindo Isabella, René ACMM Swaaij, and Miro Zeman. *Solar Energy: The physics and engineering of photovoltaic conversion, technologies and systems*. UIT Cambridge, 2015.

[4] Lewis M Fraas. History of solar cell development. In *Low-Cost Solar Electric Power*. Springer, 2014.

[5] IEC 60904-3, photovoltaic devices - part 3: Measurement principles for terrestrial photovoltaic (pv) solar devices with reference spectral irradiance data. 2008.

[6] Claudia Duran. *Bifacial solar cells: high efficiency design, characterization, modules and applications*. PhD thesis, 2012.

[7] Gaby JM Janssen, Bas B Van Aken, Anna J Carr, and Agnes A Mewe. Outdoor performance of bifacial modules by measurements and modelling. *Energy Procedia*, 77:364–373, 2015.

[8] *ITRPV, 11th Edition*. 2020. https://itrpv.vdma.org/download.

[9] PV Education. Heat generation in pv modules, 2021. URL https://www.pveducation.org/pvcdrom/modules-and-arrays/heat-generation-in-pv-modules.

[10] PV Education. Solar cell parameters - I-V curve, 2021. URL https://www.pveducation.org/pvcdrom/solar-cell-operation/iv-curve.

[11] Pushpendu Dwivedi, K Sudhakar, Archana Soni, E Solomin, and I Kirpichnikova. Advanced cooling techniques of pv modules: A state of art. *Case Studies in Thermal Engineering*, 21, 2020.

[12] Hesan Ziar, Bjorn Prudon, Fen-Yu Lin, Bart Roeffen, Dennis Heijkoop, Tim Stark, Sven Teurlincx, Lisette de Senerpont Domis, Elias Garcia Goma, Julen Garro Extebarria, et al. Innovative floating bifacial photovoltaic solutions for inland water areas. *Progress in Photovoltaics: Research and Applications*, 2020.

[13] Mario Verheijen. Thermal management of photovoltaics using phase change materials. 2019.

[14] G T.K. and V Raj. Use of phase change material (pcm) for the improvement of thermal performance of cold storage. *MOJ Curr. Res. Rev.*, 1:49–61, 2018.

[15] SS Chandel and Tanya Agarwal. Review of cooling techniques using phase change materials for enhancing efficiency of photovoltaic power systems. *Renewable and Sustainable Energy Reviews*, 73:1342–1351, 2017.

[16] Amir Hossein Shiravi and Mohammad Firoozzadeh. Thermodynamic and environmental assessment of mounting fin at the back surface of photovoltaic panels. *Journal of Applied and Computational Mechanics*, page 3, 2020.

[17] COOLBACK Company B.V. URL https://www.coolback.com/. Access date March 10, 2021.

[18] LG. The next evolution leap. LG NeON^{TM} 2 Bifacial, 2016. URL https://www.zonnepanelen.net/nl/pdf/panels/lg-neon-2-bifacial-4.pdf.

[19] Malte Ruben Vogt, Henning Schulte-Huxel, Matthias Offer, Susanne Blankemeyer, Robert Witteck, Marc Köntges, Karsten Bothe, and Rolf Brendel. Reduced module operating temperature and increased yield of modules with perc instead of al-bsf solar cells. *IEEE Journal of Photovoltaics*, 7(1):44–50, 2016.

[20] M. Rubin. Optical properties of soda lime silica glasses. *Solar energy materials*, 12(4):275–288, 1985.

[21] Bertrand Girardin, Gaëlle Fontaine, Sophie Duquesne, Michael Försth, and Serge Bourbigot. Characterization of thermo-physical properties of eva/ath: application to gasification experiments and pyrolysis modeling. *Materials*, 8(11):7837–7863, 2015.

[22] A Riverola, A Mellor, D Alonso Alvarez, L Ferre Llin, I Guarracino, CN Markides, DJ Paul, D Chemisana, and N Ekins-Daukes. Mid-infrared emissivity of crystalline silicon solar cells. *Solar Energy Materials and Solar Cells*, 174:607–615, 2018.

[23] Engineering Toolbox. Aluminum - radiation heat emissivity, 2003. URL `https://www.engineeringtoolbox.com/radiation-heat-emissivity-aluminum-d_433.html`.

[24] COMSOL. Heat transfer module user's guide, 2018. URL `https://doc.comsol.com/5.4/doc/com.comsol.help.heat/HeatTransferModuleUsersGuide.pdf`.

[25] Martin K Fuentes. A simplified thermal model for flat-plate photovoltaic arrays, 1987. Sandia National Labs., Albuquerque, NM (USA).

[26] Veikko Schepel, Arianna Tozzi, Marianne Klement, Hesan Ziar, Olindo Isabella, and Miro Zeman. The dutch pv portal 2.0: An online photovoltaic performance modeling environment for the netherlands. *Renewable Energy*, 154:175–186, 2020.

[27] Tian Shen Liang, Mauro Pravettoni, Chris Deline, Joshua S Stein, Radovan Kopecek, Jai Prakash Singh, Wei Luo, Yan Wang, Armin G Aberle, and Yong Sheng Khoo. A review of crystalline silicon bifacial photovoltaic performance characterisation and simulation. *Energy & Environmental Science*, 12(1):116–148, 2019.

[28] Solargis. Alice springs, australia. URL `https://apps.solargis.com/prospect/map?s=-23.698388,133.881289&c=-23.699354,133.88013,11`.

[29] Silvana Ayala Pelaez, Chris Deline, Sara M MacAlpine, Bill Marion, Joshua S Stein, and Raymond K Kostuk. Comparison of bifacial solar irradiance model predictions with field validation. *IEEE Journal of Photovoltaics*, 9(1):82–88, 2018.

[30] Rudi Santbergen, Tomomi Meguro, Takashi Suezaki, Gensuke Koizumi, Kenji Yamamoto, and Miro Zeman. Genpro4 optical model for solar cell simulation and its application to multijunction solar cells. *IEEE journal of photovoltaics*, 7(3):919–926, 2017.

[31] Guangtao Yang, Andrea Ingenito, Olindo Isabella, and Miro Zeman. Ibc c-si solar cells based on ion-implanted poly-silicon passivating contacts. *Solar Energy Materials and Solar Cells*, 158:84–90, 2016.

[32] Ismail Kaaya, Michael Koehl, Amantin Panos Mehilli, Sidrach de Cardona Mariano, and Karl Anders Weiss. Modeling outdoor service lifetime prediction of pv modules: effects of combined climatic stressors on pv module power degradation. *IEEE Journal of Photovoltaics*, 9(4):1105–1112, 2019.

[33] globalpetrolprices.com. Australia fuel prices, electricity prices, natural gas prices. URL `https://www.globalpetrolprices.com/Australia/`. Access date March 3, 2021.